EFFECTS OF DEPOSITIONAL ENVIRONMENT, ASSSEMBLAGE TAPHONOMY AND DIAGENESIS ON VERTEBRATE SKELETAL PRESERVATION IN A CREVASSE SPLAY SANDSTONE, UPPER CRETACEOUS HELL CREEK FORMATION, EASTERN MONTANA

by

Daigo Yamamura

A thesis submitted in partial fulfillment
of the requirements for the degree

of

Master of Science

in

Earth Sciences

MONTANA STATE UNIVERSITY
Bozeman, Montana

May, 2013

©COPYRIGHT

by

Daigo Yamamura

2013

All Rights Reserved

APPROVAL

of a thesis submitted by

Daigo Yamamura

This thesis has been read by each member of the thesis committee and has been found to be satisfactory regarding content, English usage, format, citation, bibliographic style, and consistency and is ready for submission to The Graduate School.

James G. Schmitt

Approved for the Department of Earth Sciences

David W. Mogk

Approved for The Graduate School

Dr. Ronald W. Larsen

STATEMENT OF PERMISSION TO USE

In presenting this thesis in partial fulfillment of the requirements for a master's degree at Montana State University, I agree that the Library shall make it available to borrowers under rules of the Library.

If I have indicated my intention to copyright this thesis by including a copyright notice page, copying is allowable only for scholarly purposes, consistent with "fair use" as prescribed in the U.S. Copyright Law. Requests for permission for extended quotation from or reproduction of this thesis in whole or in parts may be granted only by the copyright holder.

Daigo Yamamura

May 2013

ACKNOWLEDGEMENTS

This research is partially funded by the Geological Society of America, Departments of Earth Science and Ecology of Montana State University. I would like to thank Jim Schmitt for advising this project. I would like to thank Dave Mogk for teaching me SEM, XRD and CL operations and interpretation of these data. I would like to thank Dave Varricchio for teaching me paleontological and taphonomic data collection/interpretation. I would also like to thank Frankie Jackson for fieldwork arrangement, Takuya Imai and MSSE field paleontology students for field assistance. I would like to thank Department of Ecology (especially Dave Willey) for assigning a graduate teaching assistant position for seven consecutive semesters. Last, I would like to thank my family for inspiration and support.

TABLE OF CONTENTS

1. INTRODUCTION 1

Location and Geologic Setting 5
Faunal Composition of the Assemblage 9

2. MATERIALS AND METHODS 11

Fieldwork 11
Materials for Microscopy and X-ray Analysis 13
Rock Samples 13
Fossil Samples 14
Microscopic Observation/Analyses 15
Petrography 15
Optical Cathodoluminescence (CL) Microscopy 16
Scanning Electron Microscopy (SEM) 17
X-Ray Diffraction 18

3. LITHOFACIES 21

Trough Cross-stratified Sandstone (Lithofacies: St) 23
Interpretation 23
Massive Sandstone (Lithofacies: Sm) 24
Interpretation 25
Massive Mudrock (Lithofacies: Fm) 25
Interpretation 26
Interlaminated very fine-grained sandstone and mudrock (lithofacies: Fl) 26
Interpretation 27
Lignitic Coal (lithofacies: C) 27
Interpretation 27
Facies Association 28
Facies Association 1 28
Interpretation 30
Facies Association 2 31
Interpretation 31
Overall Interpretation 32

4. RESULTS 33

Taphonomy 33
Petrography 35
Basal Sandstone 35
Bone-bearing Sandstone 37

TABLE OF CONTENTS - CONTINUED

Concretion....38
Bones....43
Cathodoluminescence....45
Basal Sandstone....47
Bone-bearing Sandstone....47
Concretion....47
Scanning Electron Microscopy....48
Bone-bearing Sandstone....48
Concretion....49
Bones....52
X-ray Diffraction....54
Full Range (10-70°) Scan....55
Basal Sandstone....55
Bone-bearing Sandstone....56
Concretion....56
Bone....56
Clay Mineral Analysis....57
Basal Sandstone....57
Bone-bearing Sandstone....58
Concretion....59

5. DISCUSSION....61

Taphonomy....61
Sorting and Orientation....61
Bone Modification....62
Diagenesis....62
Diagenetic Processes Recorded....62
Basal Sandstone....62
Bone-Bearing Sandstone....65
Fossil Bones....67
Mechanical Effect of Compaction....68
Burial Depth....69
Bone Microstructure....71
Alteration of Bone Minerals....73
X-Ray Diffraction....74
Fossil Color....74
Authigenic Mineral Precipitation....75
Siderite....76
Clay Minerals....76
Barite....77
Hematite....78

TABLE OF CONTENTS - CONTINUED

Geochemistry of Pore-Fluids 78
Pedogenesis 79
Eogenesis 81
Mesogenesis 82
Telogenesis 83
Digenetic Microenvironment within Fossilized Bones 84

6. CONCLUSION 85

Future Study 86

REFERENCES CITED 88

APPENDICES 96

APPENDIX A: The Map of Fragments of the Femur Sample 97
APPENDIX B: The List of Treatment and Description of Thin-sections 99

LIST OF TABLES

Table Page

1. Lithofacies classification in this study 21

2. Taphonomic Data 33

3. Diagenetic stage 81

LIST OF FIGURES

Figure Page

1. Map of study area and major geologic features 6

2. Stratigraphic column of the study area 7

3. Map of Glendive, MT and study site 9

4. Field photograph and a map of the quarry 12

5. Field photograph of the outcrop studied 13

6. Field photographs of lithofacies.....22

7. Stratigraphic column of the outcrop 29

8. Photograph of a bone fragment with possible bitemarks.....35

9. Photomicrographs of the basal sandstone 36

10. Photomicrographs of the bone-bearing sandstone 37

11. Schematic diagram of bone and concretion spatial relation 39

12. Photomicrographs of the concretion near the boundary 40

13. Photomicrographs of the concretionary matrices 41

14. Photomicrographs of the grains included in concretion 42

15. Picture and micrographs of the femur.....43

16. Photomicrographs of the fossil bones.....44

17. Cathodoluminescence micrographs of the rocks 46

18. SEM micrograph and EDS spectra of the bone-bearing sandstone 49

19. SEM micrograph and EDS spectra of a quartz grain in the concretion.....50

20. SEM micrograph and EDS spectra of a fractured quartz grain 51

LIST OF FIGURES - CONTINUED

Figure Page

21. SEM micrograph and EDS spectra of a feldspar grain in the concretion 52

22. SEM micrograph and EDS spectra of a Haversian canal in the femur 53

23. Elemental map of the fossil bone 54

24. Full range XRD spectra of rock samples 55

25. Full range XRD spectra of fossil bones 56

26. Clay range XRD spectra of the basal sandstone 57

27. Clay range XRD spectra of the bone-bearing sandstone 59

28. Clay range XRD spectra of the concretion 60

29. Schematic diagram for burial depth and porosity relationship 70

30. Schematic diagram for the voids in bones 76

31. Paragenetic sequence for the fossils and rocks 80

ABSTRACT

Although a great deal of paleontological information is derived from analyzing fossilized skeletal remains, the fossilization process of vertebrate skeletal remains is poorly understood. Depositional environment, taphonomy and diagenesis of an assemblage of vertebrate skeletal elements from a sandstone in the Late Cretaceous Hell Creek Formation are investigated in order to decipher relations between sandstone diagenesis and skeletal element fossilization. Fieldwork included taphonomic data collection, section measurement and description as well as sample collection. The rock and fossil bone samples were analyzed by petrography, cathodoluminescence, scanning electron microscopy (SEM) and X-ray diffractometry (XRD).

The depositional environment including the fossil assemblage is interpreted as a crevasse splay based on the facies association of repeating sequences of mudrock and fine sandstone overlying channel and levee deposits. Taphonomic data suggest the bones were exposed on the surface up to 15 years before burial, and the assemblage is time-averaged. Although sandstone including the fossil bones indicates physical compaction, fossil bones do not exhibit signs of compaction. Barite is an unusual authigenic mineral found in fossil bones, suggesting collagen degradation during early diagenesis facilitated unique diagenetic microenvironment within bones. Calcite and siderite cements were precipitated multiple times, suggesting alkaline pore-fluid conditions were common during diagenesis. However, oversized pores and highly altered grains indicate that porefluids were acidic during late diagenesis; acidic pore-fluid conditions are likely due to the organic acid produced by degradation of organic molecule at higher diagenetic temperatures. Fossil bone minerals are altered due to 1) early pore-fluid infiltration combined with dehydration/rehydration processes, 2) saline pore-fluid infiltration and 3) increased temperature and pressure during deeper burial.

This study demonstrates that petrography, XRD and SEM/EDS together can help decipher the diagenetic history of fossilized bones. In order to maximize the information, not only the fossil bones, but surrounding rocks need to be analyzed because surrounding rocks record different sets of diagenetic processes such as calcite precipitation in the vadose zone, siderite precipitation in the phreatic zones, acidic pore-fluid condition during mesogenesis.

INTRODUCTION

Fossilized remains of organisms in the geologic record provide an excellent opportunity for studying extinct organisms from individual level (e.g. biomechanics) to global scale (e.g. mass extinction). However, the fossil record is highly biased mainly due to 1) differing durabilities of biological materials, 2) the depositional environment and 3) post-depositional diagenetic environment (Kidwell, 2003). Thus, investigating the sources of such bias has become an important subject within paleontology.

Despite their large skeletal mass, terrestrial vertebrates provided less total biomass to the fossil record than plants or invertebrates due to small populations and high mobility (Behrensmeyer, 2003). Thus, preserving a concentration of vertebrate skeletal remains requires particular taphonomic processes (Behrensmeyer, 2003). Terrestrial vertebrate remains are most common in fluvial deposits, which have multiple subenvironments (e.g. channel bar, channel fill, crevasse splay and floodplain soil) (Briggs, 2003, p. 319). Since each subenvironment has a unique mode of preservation due to rates and modes of channel aggradation and climate, investigating depositional environment is particularly important in fluvial deposits.

Taphonomy concerns any events that intervene between death and fossilization and the effects of those events on the retrieval of information about the past (Shipman, 1981, p.6). Such study includes analyzing sorting, orientation and modification (e.g. weathering and abrasion) of the skeletal remains, which in turn provides information on depositional environment such as mode of skeletal element transportation and sorting as well as biological activity affecting the skeletal remains (e.g. scavenging).

Although a great deal of paleontological information is derived from analyzing fossilized skeletal remains, the fossilization process of vertebrate skeletal remains is poorly understood. However, fossilization of vertebrate skeletal remain is presumably closely related to lithification of enclosing rocks because both rocks and fossils experience the same physical conditions such as temperature, pressure, and exposure to diagenetic fluids. Therefore, understanding lithification processes of the surrounding rock helps in deciphering the process of fossilization.

Enclosing sandstone matrix has been invoked as an entombing medium facilitating preservation of vertebrate skeletal material by isolation from contact with pore fluids (Schweitzer et al., 1997). Some studies have asserted that Upper Cretaceous Hell Creek dinosaur fossils in eastern Montana preserve extraordinary structures including endogeneous blood vessels (Schweitzer et al., 1997, 2005 and 2007; Schweitzer, 2011) and exogeneous biofilm (Kaye et al., 2008). However, none of these studies focus on the geologic processes operating on fossil preservation. Thus, studying the diagenetic history of skeletal remains in the Hell Creek Formation may shed some light on preservation of such structures.

The Upper Cretaceous Hell Creek Formation has yielded a spectacular Maastrichtian (70.6-65.5 Ma) (Walker and Geissman, 2009)) fossil record including 22 genera of dinosaurs collected over a hundred years (Johnson et al., 2002; Russel and Manabe, 2002). The Hell Creek Formation represents primarily a fluvial depositional system, and mode of preservation within the Hell Creek Formation is highly variable; for example, vertebrate remains typically do not occur in swamp deposits, and some channel

deposits have yielded articulated skeletons (Russel and Manabe, 2002). Therefore, understanding depositional environment of the fossil bearing rock is important for any further investigation.

An assemblage of vertebrate skeletal elements from a sandstone in the Hell Creek Formation provides an opportunity to investigate relations between sandstone diagenesis and skeletal element fossilization. A fossil bone assemblage was found near Glendive, MT, which contains many small and fragmentary fossils as well as three large (>30cm) bones partially exposed to the surface. Such in situ preservation allows to investigate the mineralogical characteristics of the fossil bones and surrounding rocks by limiting the effect of surface weathering. Modification of the skeletal elements can take place prior to sandstone burial, which include transportation, surface weathering and biological activities (i.e. scavenging and boring). Therefore, depositional environment and taphonomy of such assemblage need to first be investigated. The objective of this study is threefold; 1) determine the depositional environment of the sandstone entombing the fossil assemblage, 2) document the taphonomic attributes of the fossil assemblage and, 3) determine the physical/chemical diagenetic processes operating during fossilization of the vertebrate skeletal remains.

The following questions need to be addressed in order to achieve the first objective; 1) What is the lithologic characteristics (e.g. grain size and composition) of the sandstone including the fossil assemblage?; 2) What sedimentary structures are present in the sandstone including the fossil assemblage?; and 3) What is the facies association within the depositional sequence? Likewise, another set of questions needs to be

addressed to achieve the second objective; 1) Does the assemblage indicate any sorting in terms of skeletal element or size?; 2) Do the fossils show a pattern/trend in terms of bone modification (i.e. weathering, abrasion and breakage)?; and 3) Do bones have any preferred orientation?

Diagenesis comprises the post-burial physical, chemical, and biological changes to sediment and enclosed skeletal remains during lithification and fossilization (Hedges, 2002; Boggs, 2003, p. 354). Both sediment and enclosed skeletal remains have presumably experienced similar diagenetic conditions such as pressure, temperature, and pore-fluid geochemistry. Thus, determining the diagenetic pathway for the enclosing sandstone helps deciphering the diagenetic pathway for the skeletal remains. Such investigation includes analyzing modification of pore spaces/fabric and diagenetic mineral precipitation/alteration in both enclosing sandstone and skeletal remains. The hypothesized diagenetic pathway for skeletal remains includes: 1) early precipitation of carbonate to prevent physical destruction/dissolution, 2) alteration of bone mineral to more stable mineral under higher temperature and pressure conditions, and 3) modification of pore spaces in skeletal remains by compaction and precipitation of authigenic minerals. These hypotheses are tested by answering following research questions: 1) What is the mechanical effect of compaction?; 2) What is the chemistry of the pore-fluid bones were exposed to?; 3) Is bone mineral altered to other minerals?; 4) What authigenic minerals are present in fossilized bone?; and 5) Do fossils retain original microstructure? An additional question is addressed in order to consider possible isolation of skeletal remains from groundwater by early carbonate (and/or other

authigenic mineral) precipitation; 6) Is there any sign of different diagenetic fluid conditions between fossilized bone and surrounding sandstone (i.e. separation of diagenetic microenvironment)?

Location and Geologic Setting

The Upper Cretaceous Hell Creek and overlying Paleocene Tullock (or Fort Union) Formations formed as a prograding wedge of clastic sediment associated with the retreat of the Western Interior Seaway (Belt et al., 1984; Fastovsky, 1987). The stratigraphic position of the fossil assemblage and sedimentary sequence in this study is 30-40m below the K-Pg (or traditionally called K-T) boundary (Figure 2). The Hell Creek Formation overlies the Colgate Member of the Fox Hills Sandstone (Bishop, 1973; Johnson and Hickey, 1990) and the upper boundary of the Hell Creek Formation (K-Pg boundary) is defined by the stratigraphically lowest lignite bed above the highest in situ dinosaur remains (Brown, 1952). The Hell Creek Formation sediments are volcaniclastic sediments derived from the Cordilleran highland to the West (Zaleha, 1988). The estimated duration of deposition represented by the Hell Creek Formation varies from 1.36 to 2.5 million years (Johnson and Nichols, 1990; Hicks et al., 2002; Lund et al., 2002).

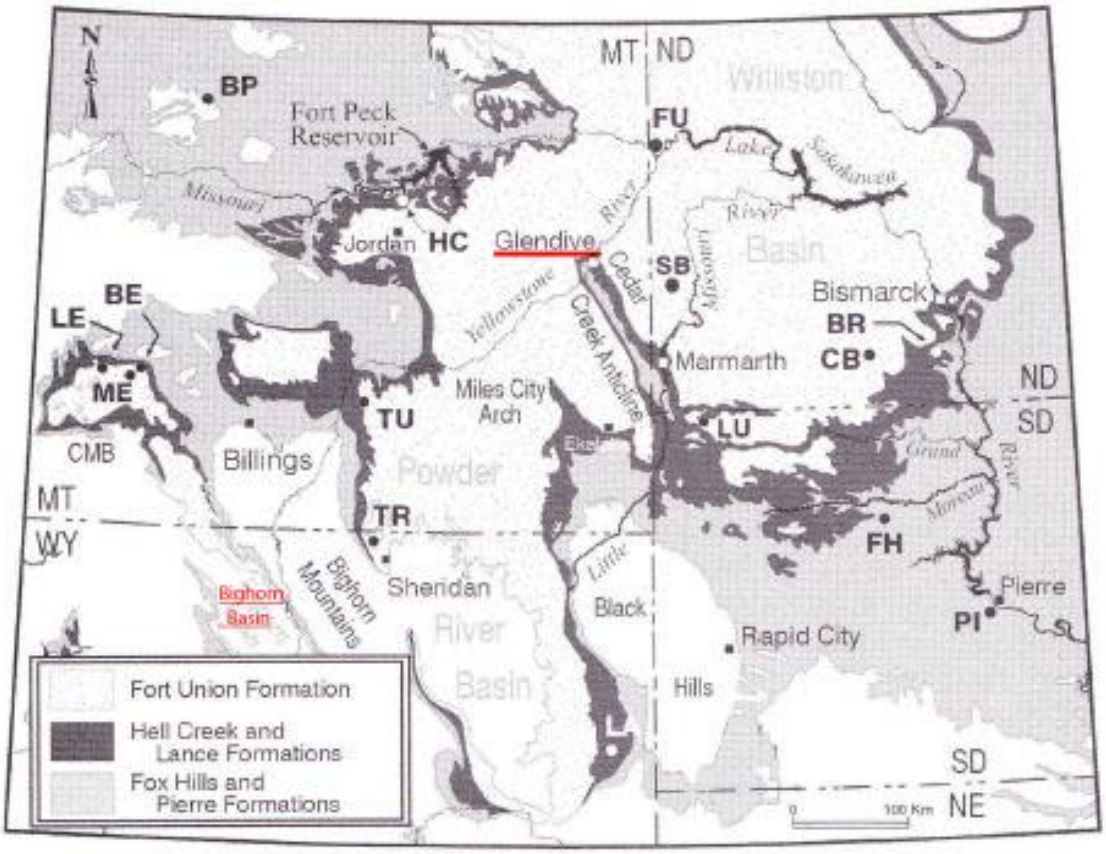


Figure 1. Regional map showing location of Glendive, major geologic features, and exposed formations (modified from Hartman, 2002).

The fossil assemblage for this study was found in Makoshika State Park near Glendive, Montana. Glendive is located near the western border of the Williston basin and northwestern flank of Cedar Creek anticline (Figure 1). The K-Pg boundary is well-exposed near the Kinney Coulee trail in Makoshika State Park.

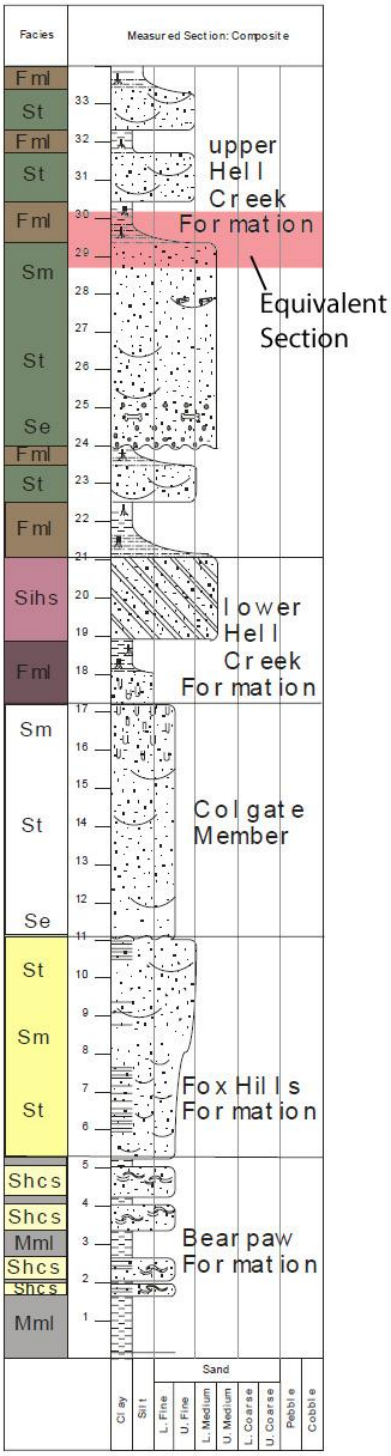
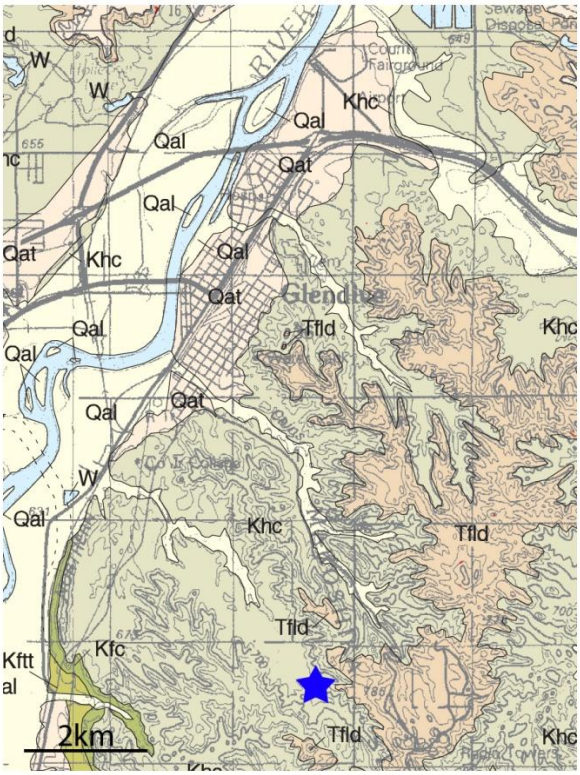


Figure 2. The Hell Creek Formation and adjacent rock units in study area (modified from Flight, 2004). Section labeled as "Equivalent section" is stratigraphic equivalent to the section in this study.

Zaleha (1988) states 1) the Hell Creek Formation in this area is composed of interbedded floodplain mudrock and channel sandstone and 2) lithofacies observed in the study area are comparable to the five lithofacies described by Fastovsky (1987), which were later expanded to nine lithofaices by Sheehan et al. (1991).

The fossil assemblage that is the focus of this study was found approximately 1.5 km east of the Caprock trailhead in Makoshika State Park, near Glendive, Montana and is 2.5 km southeast of the end of Parkview Drive (GPS coordinate: 47°03'26.98"N, 104°41'35.83"). Three large dinosaur fossils (a hadrosaur humerus, rib and femur fragment of unknown dinosaur) were partially exposed along with many fragmentary and small fossils including gar scales, turtle shell, tooth fragments and unidentifiable pieces. Some fossils were partially covered by reddish brown concretions. The fossil assemblage is located straigraphically about 30-40m below the K-Pg boundary based on the topographic map (Figure 3) and field observation. The outcrop consists of a trough cross-stratified channel sandstone overlain by massive mudrock and fine-grained mud-rich sandstone beds, one of which includes the fossil assemblage. The channel sandstone and sandstone bearing the fossil assemblage will be referred as "basal sandstone" and "bone-bearing sandstone" respectively, for the remainder of this thesis.



MAP UNITS

Qal	Alluvium of modern channels and flood plains	Kfc	Colgate Member of Fox Hills Formation
Qat	Alluvium of alluvial terrace deposit	Kftt	Timber Lake Member and Trail City Member of Fox Hills Formation, undivided
Tfld	Ludlow Member of Fort Union Formation		
Khc	Hell Creek Formation		

Figure 3. Geologic map of Glendive, MT area (modified from Vuke and Colton, 1998). The blue star indicates the location of outcrop studied. Contour interval on the geologic map is 20m.

Faunal Composition of the Assemblage

The fossils found indicate this assemblage include hadrosaur (ossified tendon and humerus), ceratopsian dinosaur (hone core and teeth), small theropod dinosaur (teeth), champsosaur (femur), turtle (shell fragments, phalange and vertebra), crocodile (scute

and teeth), gar (scale) and bird (metatarsals). The assemblage also includes a gastropod cast, partially coalified pine cone and leaf impressions.

MATERIALS AND METHODS

Fieldwork

The majority of fieldwork was completed in May and July 2010. Fieldwork included taphonomic data collection, section measurement and description as well as sample collection. Taphonomic data and section measurement are important for interpreting depositional environment, which controls initial modification of bones (weathering and abrasion) and interaction with sediments.

Survey was conducted in the field first in order to locate in situ fossil assemblage. In situ fossils are important for this study because surface weathering may alter the mineralogy of the fossil bone and permineralllizing minerals. In order to maximize taphonomic data, the fossil assemblage including the most fossils was chosen as main focus of this study. The positions and orientations of fossils were recorded using 1 x 1 m grid (Figure 4) in order to determine whether fossils have preferred orientation. The weathering and abrasion/breakage of each bone were also recorded to determine whether fossils have trend in terms of bone modification.

The section measurement included trenching near the quarry for better lithologic observation (i.e. rock type, sedimentary structures, etc.) and thickness measurement of each unit. Views of the trench and quarry are shown in Figure 5. Rock samples were collected at 5-10 cm deep in the quarry and basal sandstone in order to minimize the effect of surface weathering. Large fossil bones were jacketed with plaster, and vinac (vinyl acetate) was applied to keep the flaking pieces together.

Additional fieldwork conducted in July 2011 and July 2012 included prospecting adjacent areas and searching for other fossils in the quarry. Taphonomic data were not collected during this additional fieldwork.

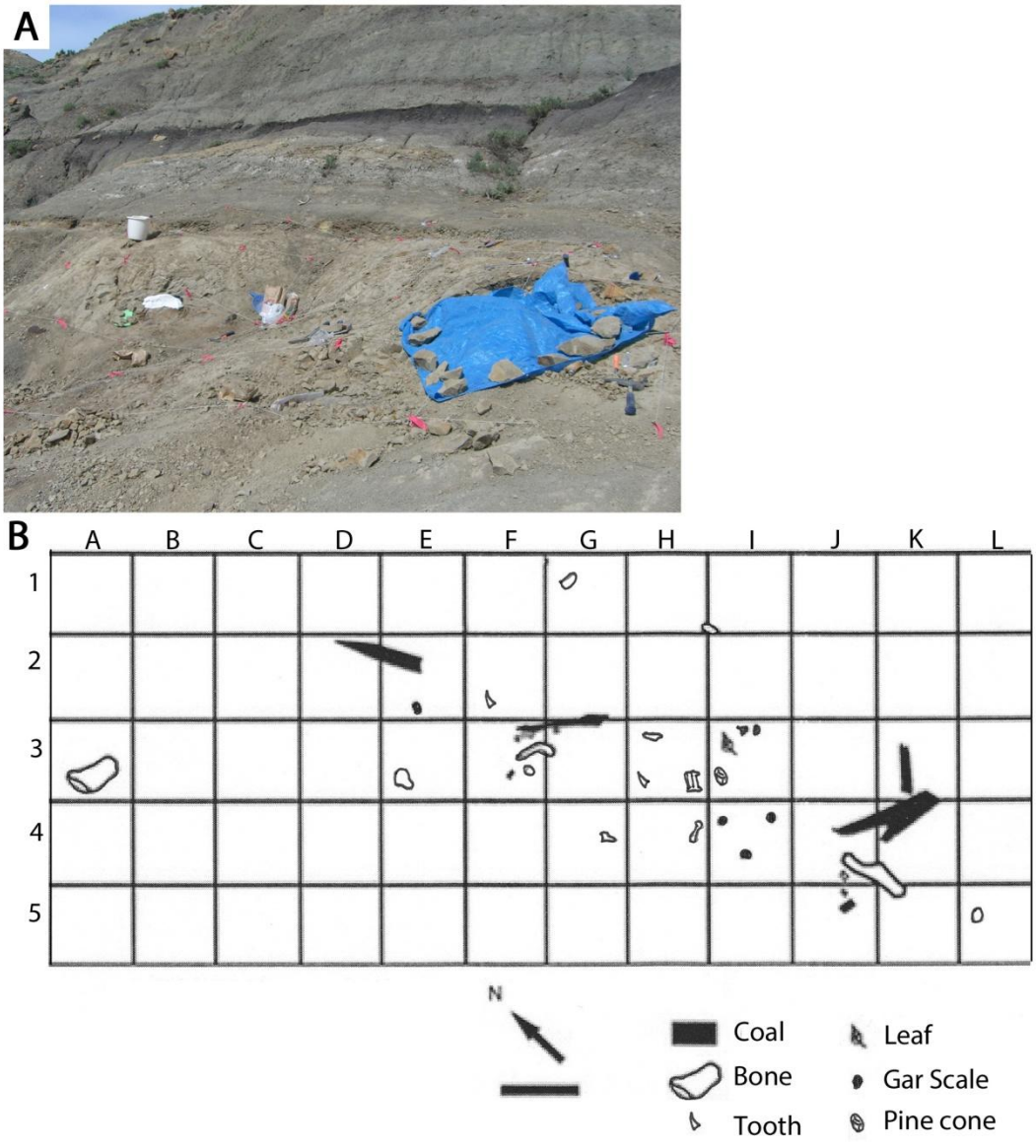


Figure 4. A) Field photograph showing grid on the quarry. Large humerus is under the blue sheet. Pink tape was attached to each nail for ease of viewing grids. B) Map of the quarry from 2010 excavation, which only includes in situ fossils and coal.

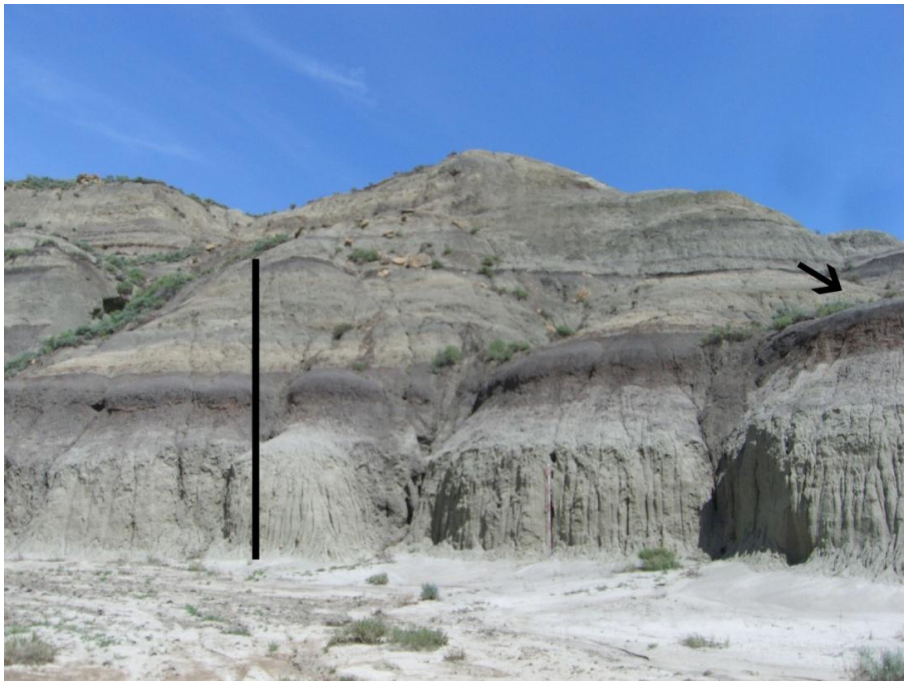


Figure 5. The outcrop including the views of trench and quarry. The thick line indicates the area for trenching, and an arrow locates the quarry. The distance between the quarry and measured section is about 10m.

Materials for Microscopy and X-ray Analysis

Rock Samples

Rock samples collected include 1) the basal sandstone, 2) bone-bearing sandstone and 3) concretions. The basal and bone-bearing sandstone samples (approximately 3 x 5 x 5 cm fragments) were collected after removing 5cm of the exposed portion in order to avoid possible alteration by surface weathering. The concretion samples (two fragments from each) were collected from concretions formed on the outer surface of a humerus of a large hadrosaur and a rib fragment of an unknown dinosaur during fossil preparation. These concretions exhibit similarity in terms of color, fabric and enclosed grains. Thin-section samples of concretions are subdivided into three groups; 1) concretion in direct

contact with bone (either inside or outside), 2) close (within a few mm to 1 cm) to bones and 3) away from the bones (up to 3cm).

Fossil Samples

Fossil samples include the femur and rib fragments of an unknown dinosaur. Both fossil fragments were only partially exposed at the time of discovery. Since microscopy and X-ray analyses require destructive preparation, the hadrosaur humerus was excluded. The fossil fragments are reddish brown in color, and their exposed surface weathers to white-tan color. Concretions are present on the surface and inside of both the femur and rib fragments, but smaller pores (e.g. Haversian canal) are not permineralized.

Fossil samples were too friable to cut with a rock saw. However, the femur fragment was too large to ship for professional preparation. Thus, the femur fragment was jacketed with fiber glass and plaster and covered with duct tape in order to prevent further breakage while sawing. Unfortunately, the femur fragment broke apart into smaller pieces while being cut using a rock saw. Thus, each fragment selected for thin-section was mapped in order to record the proximity to the center of the bone (Appendix A). Additionally, all the samples for thin-section analyses were taken from the parts where vinac was absent. Each thin-section plane was cut roughly perpendicular to the shaft of the femur (i.e. transverse sections). Another set of bone samples for thin-section were also taken from the middle section of rib fragment where the concretion was still attached and vinac was absent.

Microscopic Observation/Analyses

The microscopic analyses included thin-section petrography, optical cathodoluminescence (CL) microscopy, and scanning electron microscopy (SEM). Additionally, energy dispersive spectrometry (EDS) was utilized during SEM sessions in order to analyze elemental composition of grains and cements. Thin-section microscopy was used to observe the characteristics of grains, open spaces (geometry and distribution) and fabric. Optical CL was utilized to differentiate various generations of carbonate cementation and grain alteration in sandstone and concretion samples. SEM/EDS was utilized for finer scale observation of grain coatings and microstructures in fossil bones as well as elemental composition analyses of the precipitates in open spaces.

Petrography

Petrography was used to identify the grain types. The characteristics of grains (e.g. alteration, dissolution, and overgrowth) observed with thin-section petrography provides information on mechanical effect of compaction and pore-fluid geochemistry affecting the rock and fossil. The characteristics of grains are also important for determining the need for additional analyses such as CL and SEM/EDS. The observation of pore spaces by petrography also provides information on mechanical effects as well as precipitation/dissolution of minerals, which in turn helps deciphering the pore-fluid geochemistry. The grains and fabric observed with petrography provides information on the mechanical effect of compaction.

After sorting and initial preparation, fossil and rock samples were sent to Spectrum Petrographics Inc. for professional thin-section preparation. In case further analyses were necessary, thin-sections were not covered with cover slides. Some rock samples were stained for compositional analysis; K-feldspar stain for sandstone samples and calcite and Fe-carbonate stains for concretion samples. Furthermore, unstained sections were polished for CL. List of treatment and description of each thin-section is provided in Appendix B.

A petrographic microscope (Nikon Eclipse LV 100 POL) equipped with objective lenses (2, 10, 20, 40, and 60x), an ocular (10x), and a camera unit (Nikon, DS-5 Mc) was used for primary microscopic observation of grains, pores/fabric and cementation of rock samples as well as fabric, open space and permineralization/mineral precipitation in fossil samples. Photomicrographs were taken with the camera unit and DS-L1 unit; resolution used for photomicrograph was 2560 x 1920 pixels. Thin sections were marked with India ink when additional observations/analyses with CL and SEM are necessary.

Optical Cathodoluminescence (CL) Microscopy

Optical cathodoluminescence (CL) microscopy was used on polished thin-sections to distinguish different generations of carbonate minerals (e.g. calcite), which in turn helps deciphering geochemistry of pore-fluid that both sandstones and fossils were exposed to throughout the diagenesis. A luminoscope (Relion Industries, Model ELM-2A specimen chamber) with rotary vane pump (Pascal 2005SD by Alcatel inc.) and a control box (Relion Industries, Reliontron control box coupled with Duniway Stockroom Corp., Terranova model 924A thermocouple vacuum gauge) were attached to a

petrographic microscope (Nikon, eclipse 50i) for optical CL. Acceleration voltage was kept at -8.8kV. Chamber pressure was maintained at around 100mTorr for optimum CL signals. Photomicrographs were taken with 4x objective lens and Nikon DS-2Mv and DS-L1 units attached to the microscope. The resolution used for the photomicrographs was 1600 x 1200 pixels.

Scanning Electron Microscopy (SEM)

The scanning electron microscope (SEM; JEOL 6100, housed at the Image and Chemical Analysis Laboratory) was utilized for finer scale observation of the grains and matrices in sandstones and concretions, mineral precipitates within pores of the fossil bones and the grain coating preserved in concretions. Additionally, EDS was utilized for elemental composition analysis in order to identify mineral phases, which in turn helped deciphering authigenic mineral precipitation and pore-fluid geochemistry. The microstructures in fossil bone and grain coating in concretion selected for SEM observation were selected using the results on the thin-section microscopy and CL microscopy.

The selected thin-sections were mounted on sample holders using carbon tape and grounded with additional carbon tape and colloidal graphite, which improves micrograph image quality. The carbon coating (150 mA, 4 minutes) was used initially in order to acquire EDS without possibly problematic peaks on the spectrum. However, the iridium coating (20 mA for 30 seconds) was used later because carbon coating did not reduce charging enough to operate the SEM properly.

The JEOL JSM-6100 scanning electron microscope was operated under the following conditions: chamber pressure was kept under $8x10^{-5}$ Torr, current was set at 1.95 mA, acceleration voltage was set at 20 kV, and working distance was maintained at around 39 mm. Even though high acceleration voltage and large working distance do not produce the best image quality, a 39 mm working distance and 20 kV acceleration voltage were used in order to utilize Noran detector for energy dispersive spectrometry (EDS). SEM micrographs were taken using the software Multi-Image 2.3 (Rontec). Resolution for the micrographs was 800 x 600 pixels. EDS spectra were recorded and analyzed using software WinShell (Rontec). Most of the EDS data collection was run for 30 seconds, however, EDS data collection was run for more than three minutes for bone mineral in order to detect fluorine.

Elemental mapping was also conducted using WinShell and Multi-Image software (Rontec) with EDS FlashMap detector. The elements choseen for elemental mapping include Ca, Fe, Ba, P, F, Si and S. Resolution for the X-ray mapping used was 800 x 600 pixels. Detection time was set to 36 minutes.

X-Ray Diffraction Spectrometry (XRD)

X-ray diffraction spectrometry (XRD) was utilized for identifying mineral phases of rock and fossil samples, which in turn helps deciphering authigenic mineral and cement precipitation. Since clay minerals are major products of mineral alteration (e.g. volcanic rock fragment and feldspar), clay mineral assemblage was also analyzed using protocols from Moore and Reynolds (USGS). The identification of mineral phases in

fossil bone helps deciphering diagenetic change in mineral phases in a bone throughout diagenesis. Additionally, comparison of mineral phases in different bone fabric would help in understanding the effect of the original bone fabric on diagenetic alteration of bone minerals.

The rock samples analyzed using XRD include the basal sandstone, bone-bearing sandstone, and concretion. The basal and bone-bearing sandstone samples were selected randomly from samples (approximately 3 x 5 x 5 cm) collected in the field. A concretion sample was collected from the concretion formed on a hadrosaur humerus. The matrix of the concretion exhibits two different colors; dark reddish brown and light grey, and sample preparation only include dark colored concretion because 1) majority of the concretion is dark brown in color, 2) isolating light colored matrix from the rest of concretion was impossible.

The fossil bone samples analyzed using XRD include cortical (dense) and cancellous (spongy) portions of a femur fragment of an unknown dinosaur. The cortex bone sample was randomly selected from small fragments of femur produced during initial thin-section preparation. The cancellous bone sample was also collected from the femur; fragments with minimal concretion attachment were chosen in order to avoid skewing XRD results. Additionally, all the bone samples were collected from the parts where vinac was absent.

All rock and bone samples were ground into powders for XRD. Ground samples were put through a 63 μm sieve. Each powdered sample was mounted on a glass slide using Vaseline for random mount analysis. For the rock samples, three oriented mounts

were prepared for each rock sample by mixing with water and filtering through a 0.4μm filter paper using methods descibed in Moore and Reynolds (USGS). The oriented samples were then transferred to glass slide for further treatments. All oriented samples were air dried first. One sample from each was baked in 400°C overnight, and another was glycolated in a glycolation chamber overnight.

The X1 Advanced diffraction system (Scintag Inc.) was used with software DMSNT for XRD analyses. Acceleration voltage was set at 1.00kV with negative polarity. Random mount samples were scanned from 10° to 75° with a step-angle of 0.020°, continuous scan with a scan rate of 2.00°/minute. The random mount sample for the bone-bearing sandstone was scanned from 5° to 70° with same step-angle and scan rate. Thus, the overlapping 10°-70° range was used for further analysis. Oriented samples (air dried, baked, and glycolated) were scanned from 3 to 28° for clay mineral analysis.

The XRD data were imported to Microsoft Excel in order to edit the XRD spectra. In order to separate the spectra of different samples on a graph, an additional value was added to the count per second (CPS, the variable on y-axis). The ICDD database was used for identifying peaks. Additionally, XRD spectra were compared to known spectra when they are available on the online database Mindat (Mindat). Clay minerals were identified by comparing characteristics of the peaks (e.g. expand to larger d-spacing when glycolated and collapse to smaller d-spacing when baked) to the USGS clay mineral identification flow diagram (USGS).

LITHOFACIES

The lithofacies classification of Miall (2007, p. 79) is adopted to this study in order to avoid biased interpretation. The lithofacies and brief interpretations are summarized on Table 1. The lithofacies identified in the studied stratigraphic section include trough cross-stratified sandstone (lithofacies: St), massive sandstone (lithofacies: Sm), massive mudrock (lithofacies: Fm), interlaminated very fine-grained sandstone and mudrock (lithofacies: Fl), and coal (lithofacies: C) (Figure 6).

Table 1. Lithofacies summary for this study

Lithofacies			
Code	Facies	Sedimentary Structure	Hydrodynamic Interpretation
St	Sand, very fine to medium	Grouped trough cross-lamination	Migration of 3D dunes
Sm	Sand, very fine to fine	Massive or faint lamination	Suspension settling, bioturbated
Fl	Sand, silt, and mud	Fine wavy lamination	Suspension settling, weak traction current
Fm	Mud, silt	Massive	suspensionsettling, bioturbated
C	Coal	Plant, mud films	Standing body of water, low sediment input

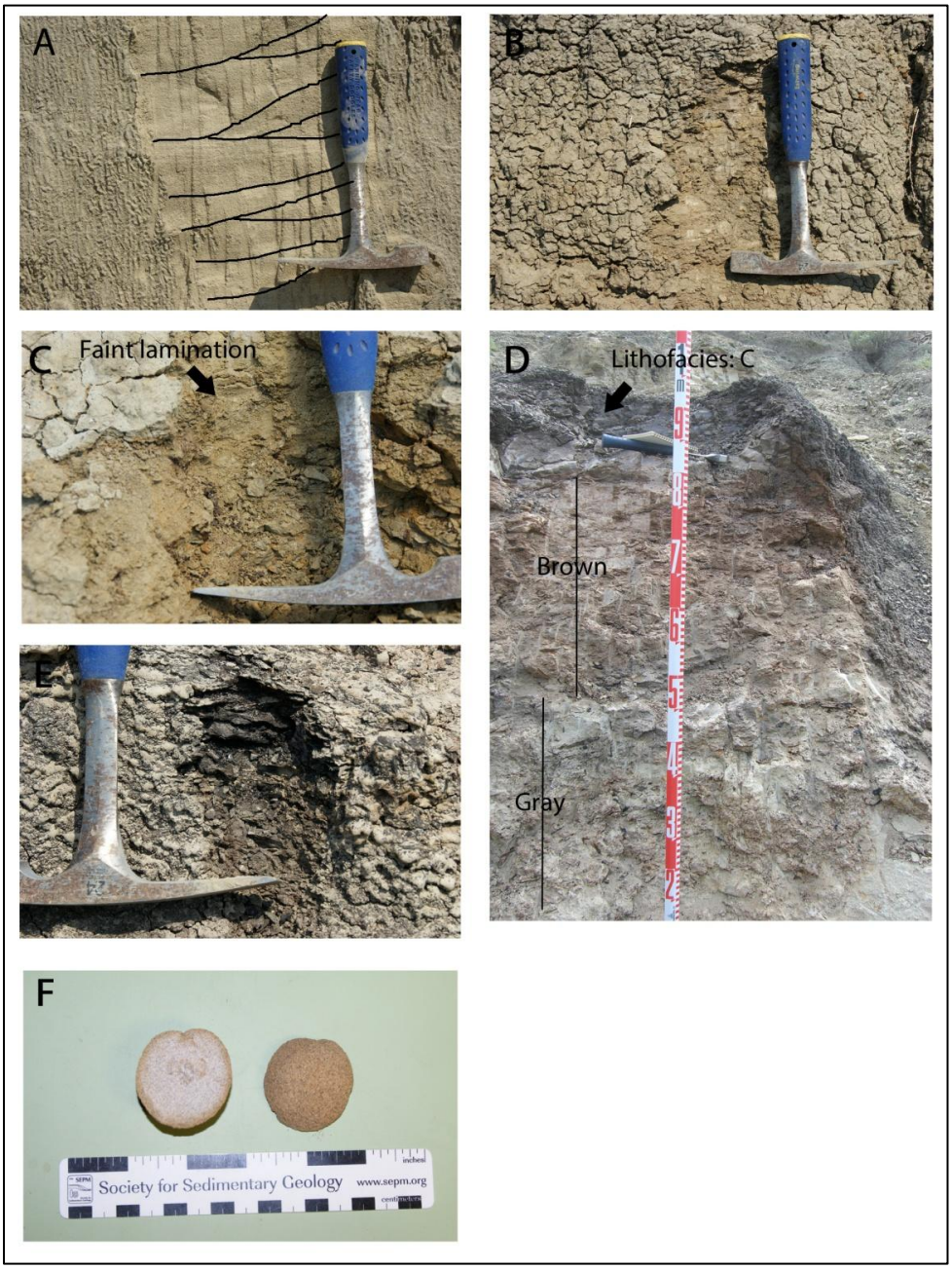


Figure 6. Five lithofacies in the study area. A) Trough cross-stratified sandstone (St); black lines were added to outline the cosets. B) Massive mudrock (Fm). C) Massive sandstone (Sm); a black arrow points to the faint lamination. D) Interlaminated very fine-grained sandstone and mudrock (Fl); includes brown and gray mud subunits. E) Coal (C); shiny lignitic coal interlaminated with dark gray mud. F) Photograph of a concretion found in the trough lithofacies St. The concretion is cut in half; left showing inside, and right showing outside. Note: Figure 6.D was taken by a different camera, which may have caused slightly different color contrast.

Trough Cross-stratified Sandstone (Lithofacies: St)

The trough cross-stratified sandstone in the study area comprises moderately sorted medium-grained sand (Figure 6.A). Grains are angular to sub-angular and include minor amounts (5-10%) of mafic minerals and volcanic rock fragments. The sedimentary structures seen in the trough cross-stratified sandstone are cosets of mutually cross-cutting troughs. The angle of trough-cross lamination ranges from 5 to 20°. The thickness of each stratification is about 2mm, and thickness of cosets ranges from 15 to 30cm. Additionally, the trough cross-stratified sandstone is grain-supported with tangential grain contacts, highly porous and very friable.

Discrete coal stringers mm's to cm's in thickness and up to 50cm in length are present. The coal stringers are oriented along the slope of trough cross-lamination. The trough cross-stratified sandstone also includes small (1-5cm) spheroidal bodies; some are friable and yellow to tan in color, and others are well cemented and reddish brown in color (i.e. concretion). Such cemented bodies however exhibit light gray color on freshly broken surfaces (Figure 6.F) and broken surfaces react with an acid (0.1M HCl). Vertebrate fossils were absent in the trough cross-stratified sandstone in the outcrop studied. Presence of trough cross-stratified sandstone beds is very common in sandstone units throughout the study area and each bed is laterally discontinuous.

Interpretation

Trough cross-stratification is formed by migration of 3D dunes, which develop under lower flow regime conditions (Harms et al., 1982). Based on their orientation, the

coal stringers represent plant material deposited on the lee side of dunes. Since original depositional structure (i.e. cross-stratification) is observed in the spheroidal bodies, both friable and well-cemented spheroidal bodies are likely products diagenesis. The absence of vertebrate remains in the basal sandstone may not have any significance since other cross-stratified sandstone beds in the study area yield fossils.

Massive Sandstone (Lithofacies: Sm)

Massive sandstone in the study area comprises poorly sorted fine- to very fine-grained sand and mud (Figure 6.C). Grains are sub-angluar and include minor amount (10%) of mafic minerals and volcanic rock fragment. Sedimentary structures or root casts are not preserved in the massive sandstone; only a few faint wavy laminations are observed. The color of massive sandstone is light gray to tan due to high clay content. The massive sandstones include smaller bodies of different colored matrices; the color of such bodies ranges from yellow to light brown and often have oxidized appearance.

Coal is present either as discrete fragments (up to 5 mm) or as stringers (up to cm's thick and decimeters in length). Partially coalified plant fossils (leaves and pine cones) are also present in the massive sandstone. Vertebrate fossils are only present in the massive sandstone labeled as the bone-bearing sandstone on the stratigraphic column (Figure 7). Spheroidal concretions found in the trough cross-stratified sandstone is absent in massive sandstone beds; the only concretions in the bone-bearing sandstone occur around fossil bones. Massive sandstone (Sm) beds are about 1m thick and occur

between massive mudrock (Fm) beds. Both upper and lower contacts between massive sandstone and massive mudrock are gradational.

Interpretation

The fine sand-sized grains and high mud content suggests the massive sandstone was deposited in a low energy setting. The massive sandstone beds can occur as a result from bank collapse in a small channel (Jones and Rust, 1983) or due to post depositional modification (Miall, 2007, p. 123). The massive sandstone beds do not occur adjacent to channel sandstone in this section, hence these massive sandstone beds are not likely bank collapse deposits. In contrast, presence of vertebrate fossils and coal stringers suggests post depositional modification by biological activity (i.e. bioturbation), hence massive fabric is interpreted as a result of post depositional modification. Fine sand and high mud content suggest that depositional environment was a low energy setting.

Massive Mudrock (Fm)

Massive mudrock consists of light- to dark-gray clay and silt (Figure 6.B). Sedimentary structures or root structures are not preserved in the massive mudrock; however, few faint laminations are observed in silty beds. Such laminations are rare and only partially preserved. Coal is present either as stringers (up to cm's thick and decimeters in length) or as small discrete fragments (up to 5 mm), and the coal content varies widely among the mudrock beds. Paleosols were very poorly developed in all the mudrock beds. The mudrock beds adjacent to coal beds exhibit a gradational increase in coal content toward the coal beds, which makes the contact between mudrock and coal

beds gradational. No vertebrate fossils were found in the massive mudrock beds. Bed thickness ranges from 20cm to 1m and gradually decrease in frequency toward the top of the outcrop.

Interpretation

Massive mud deposits are a result of suspension settling in a standing body of water (Miall, 1985). In a fluvial setting, massive mud is deposited on a distal floodplain during flooding or in standing pools of water such as floodplain ponds and swamps (Miall, 1985). The gray color of the mudrock and abundant plant debris are indicative of a poorly-drained overbank environment (Reading, 1996, p. 66). Partially preserved faint wavy lamination suggests ripple lamination was present prior to bioturbation. Presence of ripple lamination is indicative of lower flow regime conditions (Miall, 1977).

Interlaminated Very Fine-Grained Sandstone and Mudrock (Lithofacies: Fl)

Interlaminated very fine-grained sandstone and mudrock consists of brown to gray mudrock and very fine-grained gray sandstone (Figure 6.D). The contact between interlaminations is gradational and partly obscure. The color of mudrock in the bottom half is mostly gray with thin (up to 5cm) layers of brown mudrock, whereas mudrock in upper half is mostly brown in color. Some silty mudrock exhibits faint wavy laminations. Lithology of the sandstone is similar to other massive sandstone (lithofacies: Sm) beds; structureless gray mud-rich sandstone. Occurrence and thickness of sandstone subunits gradually decrease toward the top. Interlaminated very fine-grained sandstone and

mudrock overlies the basal trough cross-stratified sandstone (lithofacies: St) and is overlain by a coal bed.

Interpretation

Interlamination of mud and very fine sand represents deposition from suspension and from weak traction currents (Miall, 2007, p. 123). Faint wavy lamination suggests the presence of ripple cross-lamination, which is indicative of lower flow regime conditions. The color of the mudrock suggests the upper half was deposited in a well-drained environment (Reading, 1996, p. 66). Decrease in sand content toward the top may suggest a channel migration and succession toward distal flood plain environment.

Lignitic Coal (lithofacies: C)

Lignitic coal layers occur frequently in the Hell Creek and overlying Tullock Formations in the study area. Two lignitic coal beds were included in the sedimentary sequence studied and both beds are stratigraphically lower than the K-Pg boundary (Chapter 1). The lignitic coal layers are interlaminated with dark gray clay (Figure 6.E) and laterally discontinuous. Lignitic coal beds overlie lithofacies Fl and Fm with gradational contact.

Interpretation

Whereas autochthonous peats and coals directly overlie paleosols, allochthonous coals lack an associated underlying paleosol and accumulated in a body of still water as detrital organic matter or as a floating peat layer (Reading, 1996, p. 68). Since the

lignitic coal facies overlie a massive mudrock (lithofacies: Fm) and interlaminated very fine-grained sandstone and mudrock (lithofacies: Fl) in the sedimentary sequence studied, such coal facies are interpreted as a peat swamp deposit. McCabe (1984) suggested that the presence of coal indicates the presence of raised peat swamps undergoing rapid plant accumulation under humid-tropical conditions.

Facies Association

The outcrop studied consists five lithofacies; St, Sm, Fl, Fm and C. The measured section includes two facies association; facies association (FA) 1 and 2 (Figure 7). FA 1 includes lithofacies St overlain by Fl and C, whereas FA2 includes repeating sequences of lithofacies Sm and Fm.

Facies Association 1

Facies association (FA) 1 is defined by a trough cross-stratified sandstone (St) overlain by an interlaminated very fine sandstone and mudrock (Fl) and lignitic coal (C). The coal content within the lithofacies Fl gradually increase toward the top (contact between lignitic coal). The upper contact of FA 1 is marked by lignitic coal facies (C), and the contact between FA 1 and FA 2 is gradational. The lower contact of FA 1 is not exposed. The contact between lithofacies St and Fl is gradational; the lowermost lamina in the overlying lithofacies Fl consists of gray very-fine sand and silt. The sequence is 4.5m thick and fines upward into lithofacies Fl and C. Lithofacies C contains dark gray mud, which differs from the underlying mudrock (part of lithofacies: Fl). FA 1 is only present at the base of the outcrop studied.

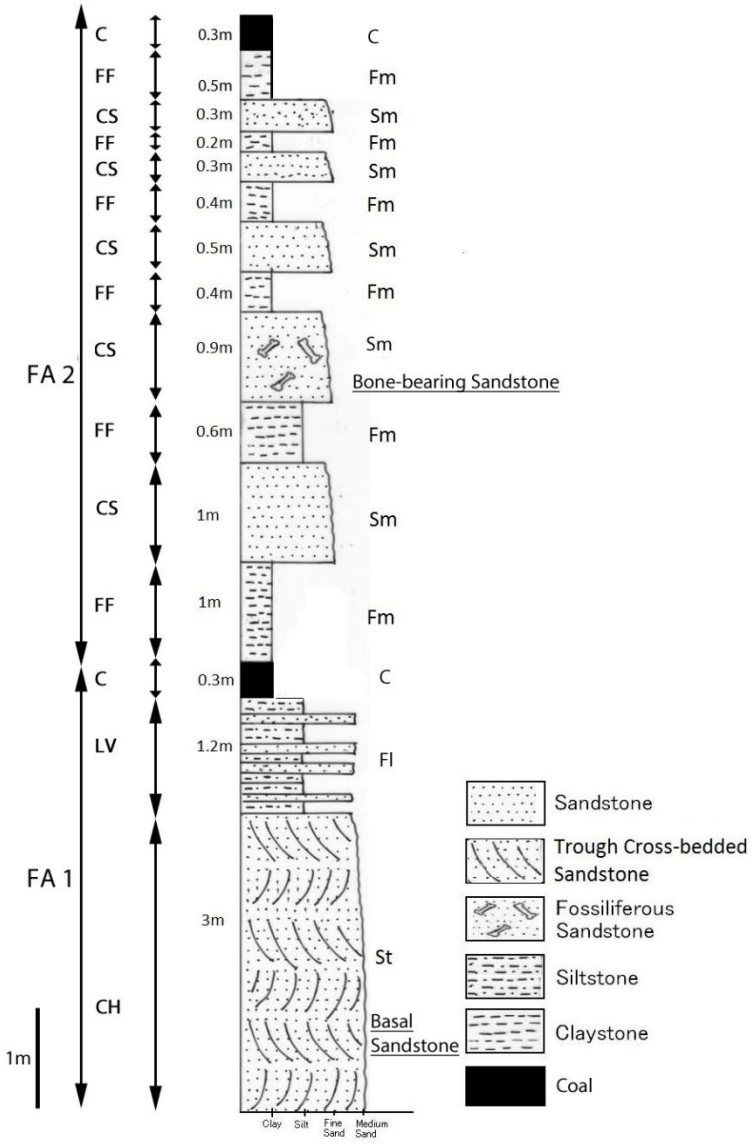


Figure 7. Stratigraphic column summarizing the lithologic characteristics of the outcrop studied. Lithofacies include trough cross-stratified sandstone (St), massive sandstone (Sm), interstratified very-fine sandstone and mudrock (Fl), massive mudrock (Fm) and coal (C). Architectural element was interpreted for each lithofacies based on the facies association: (CH), levee (LV), coal (C), floodplain fines (FF) and crevasse splay (CS). Facies association 1 (FA 1) includes channel and levee deposits whereas facies association 2 (FA 2) includes repeated sequences of crevasse splay and floodplain fine deposits.

Interpretation. Previous studies (e.g. Fastovsky, 1987; Sheehan, 1991) state the Hell Creek Formation was deposited in a fluvial setting. In a fluvial setting, migrations of 3D dunes take place in a channel (Miall, 1977), hence the cosets of lithofacies St is interpreted as a channel sandstone (architectural element CH). Although fining upward grain size and gradual contact with lithofacies Fl suggests lateral migration of the channel, further interpretation (i.e. lateral-accretion versus downstream-accretion macroform) requires additional information such as geometry of the sandstone bed. Interlaminated very fine sandstone and mudrock (lithofacies: Fl) rests directly above a channel sandstone (lithofacies: St). The gradational contact between the lithofacies Fl and St and increase in coal content within Fl suggest a gradual loss of kinetic energy in the depositional system such as channel migration or abandonment. Based on the close association with channel sandstone and gradational contact, lithofacies Fl is interpreted as a levee deposit (architectural element: LV). Lignitic coal in a fluvial deposit is interpreted as a swamp deposit (Ayres, 1986) and is indicative of a poorly drained environment. In contrast, the brown color of mud in Fl is indicative of well-drained overbank deposit (Reading, 1996, p. 66).

Based on presence of channel, levee and floodplain deposits, FA 1 is interpreted as a sequence recording channel migration. Channel migrations forming levee deposits represent sedimentary events with duration 10^2 to 10^3 years (Miall, 2007, p. 84); hence the Fl unit may represent 10^2 to 10^3 years.

Facies Association 2

Facies association (FA) 2 is defined by repeating sequences of massive sandstone (Sm) and massive mudrock (Fm). Total thickness of this sequence is 6.4m, and both top and bottom boundaries are defined by lignitic coal facies (C). Boundaries between Sm and Fm are gradational. Thickness of each bed gradually decreases toward the top of this sequence. Differential weathering due to the relatively resistant sandstone beds (Sm) produced a gentle slope in the middle of the hill. Overall sequence of the FA 2 exhibits fining upward trend in grain size.

Interpretation. Crevasse splays form lobate sheets of sand that prograde into a wetland environment and are common features of fluvial depositional system (Smith, 1983). Studies of modern anastomosing system (Smith, 1983) also indicates that multiple stacked splay sequences separated by mud are common. Therefore, FA2 is interpreted as a series of crevasse splay deposits based on presence of multiple fine-grained sandstone beds (Sm) interbedded with mudrock beds (Fm).

Crevasse splay sandstone (architectural element: CS) often exhibits trough cross-stratification or ripple cross-lamination (Miall, 2007, p. 175), and the lack of such stratifications is likely due to bioturbation suggested by the presence of plant material and fossils. Massive mudrock (Fm) can be deposited on a distal flood plain (Rust, 1978b) or in lakes from the suspended load (Castle, 1990). However, close association with crevasse splay sandstone suggests Fm was deposited on a distal floodplain (architectural element: FF).

Overall Interpretation

Local thickness of the Hell Creek Formation in the Glendive area is estimated to be 99m (Zaleha, 1988), and the Hell Creek Formation represents depositional events of 1.36 to 2.5 million years (Johnson and Nichols, 1990; Hicks et al., 2002; Lund et al., 2002). Based on these data, the 11m sequence may represent 151,000 to 278,000 years.

The overall sequence (a series of crevasse splays overlying a channel migration sequence) is interpreted as an alluvial succession from a channel to an overbank with occasional breaching of levees. Levees and crevasse splays tend to have higher rates of deposition in comparison to distal floodplain (Bridges, 2006); hence the time represented by Fm is greater where the thicknesses are comparable. Lack of paleosol horizons may suggest that sedimentary accumulation was relatively fast throughout the sequence.

RESULTS

Taphonomy

Table 2. List of fossil specimens for taphonomic analyses.

Number	Material	Taxon	grid	length	W	Abr./Break.
MSP1	humerus	Hadrosaurid	J4/K5	80	2	0/complete
MSP2	rib (partial)	Unknown Dino.	F3	30	2	0/broken
MSP3	femur (partial)	Unknown Dino.	A3	30	2	0/broken
MSP4	horn core (?)	Triceratops (?)	G1	12	2	1/broken
MSP5	tooth (fragment)	Theropod	F2	2	3	0/no root
MSP6	tooth (fragment)	Triceratops (?)	-	1	2	0/no root
MSP7	femur (head)	Champsosaurus	H4	6	3	1/broken
MSP8	ungual	Theropod (small)	-	2	1	0/complete
MSP9	phalange	Unknown Dino.	J8	15	2	0/complete
MSP10	vertebra	Theropod	F3	2.5	3	1/broken
MSP12	phalange	turtle (?)	-	0.7	1	0/complete
MSP19	vertebra	turtle (?)	-	1.5	2	0/complete

Note: Length is in centimeters. Weathering classification follows Behrensmeyer (1978), and abrasion classification follows Shipman (1981). W stands for weathering. Abr./Break. stands for abrasion and breakage.

Table 2 summarizes the fossils used in the taphonomic analysis. Even though smaller fragmentary bones are very abundant in the assemblage, identifying orientation or timing of breakage (pre- or post-burial) is very difficult. Therefore, small fragmentary fossils were excluded from the taphonomic data. Such fragmentary bones include turtle shell fragment, gar scale, ossified tendons, crocodilian scute and other unidentifiable bone fragments. Due to the nature of fossil preservation in the fossil assemblage, the statistical significance of taphonomic data is not strong (N=12). Aside from vertebrate remains, plant fossils (leaf and pine cone) and gastropod casts are present in the quarry.

Additionally, other important fossils that are not listed on the Table 2 include 1) a fragmentary bone with possible bite mark and 2) an avian metatarsal found during additional fieldwork in 2011.

Preferred orientation is not observed among the large bones (>15cm, N=4). The assemblage does not include any skull or illium, and none of the fossil bones are articulated. The size of the fossil bones ranges from 7mm (a turtle phalange) to 80cm (a hadrosaurid humerus) (mean=15.2cm, SD=23.0, variance=531.0).

Abrasion of the bone is consistently low (0-1 in Shipman's scale; N=12, mean=1.25, SD=0.45, variance=0.20). However, weathering varies from 1-3 in Behrensmeyer's scale (N=12, mean=2.08, SD=0.67, variance=0.45). Breakage is common in this assemblage regardless of the size of the bone. Among larger bones (>15cm, N=4), two are broken and two others are nearly complete. Likewise among the smaller bones (<15cm, N=5), two are broken and three others are nearly complete. MSP4 was excluded from smaller bone group since the actual size of this bone may exceed 15cm.

One bone fragment exhibits possible bite marks (Figure 8): a series of elliptical holes partially filled with reddish brown concretion (possibly hematite). Major axes of the holes range from 1 to 1.5cm, and depth is unknown. One side (left on the Figure 8) of these holes is consistently deeper, suggesting these holes are slanted.



Figure 8. Photograph of possible bite-marks on a bone fragment. Each hole is partially filled with reddish brown concretion. The major axes of elliptical holes are parallel to the others, and the holes are partially filled with hematite concretion.

Petrography

Basal Sandstone

The stained thin-sections (Figure 9.C) exhibit up to 25% of feldspar content. Also, lithic fragments are very common (up to 30%) in the basal sandstone (Figure 9.C). Thus, the basal sandstone is a highly porous (up to 50%) feldspathic litharenite. Framework grains include quartz, feldspar, volcanic rock fragments, and accessory minerals including biotite, apatite, and other mafic minerals. Grains are subangular to angular, and some quartz grains show overgrowths.

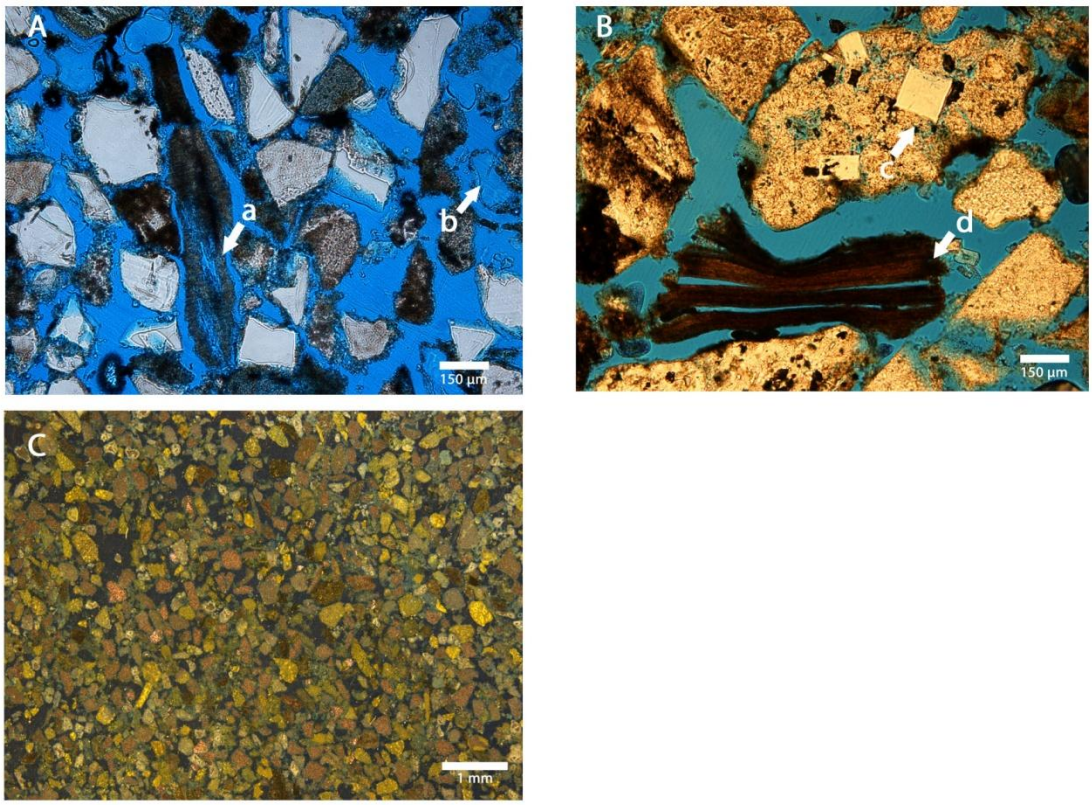


Figure 9. Photomicrographs of basal sandstone (A and B: 10x (objective lens), scale bar = 150µm and plain polarlized light (PPL); C: 2x, scale bar = 1mm and PPL with low light condition). Blue epoxy was used to recognize plucked grains versus pore space. Characteristic features shown on A and B include; a) a skeletonized grain; b) complete grain dissolution outlined by clay precipitation prior to dissolution; c) volcanic rock fragment enclosing euhedral crystals of K-feldspar; d) exploded fabric of biotite crystals. C) Lower light condition was used for better resolution of the picture. The yellow grains are stained by K-feldspar stain.

Grain contacts are point-contact to almost floating due to grain dissolution. Feldspar grains and volcanic rock fragments are highly altered; skeletonized grains (partial dissolution, Figure 9.A-a) and oversized pores (complete dissolution, Figure 9.A-b) are common. The oversized pores are often outlined by clay minerals. Some unaltered euhedral potassium feldspar crystals are present in the basal sandstone (Figure 9.B). These euhedral potassium feldspar grains are found either within or adjacent to volcanic

rock fragments. The exploded fabric of biotite (Figure 9.B-d) indicates early precipitation of calcite.

Bone-Bearing Sandstone

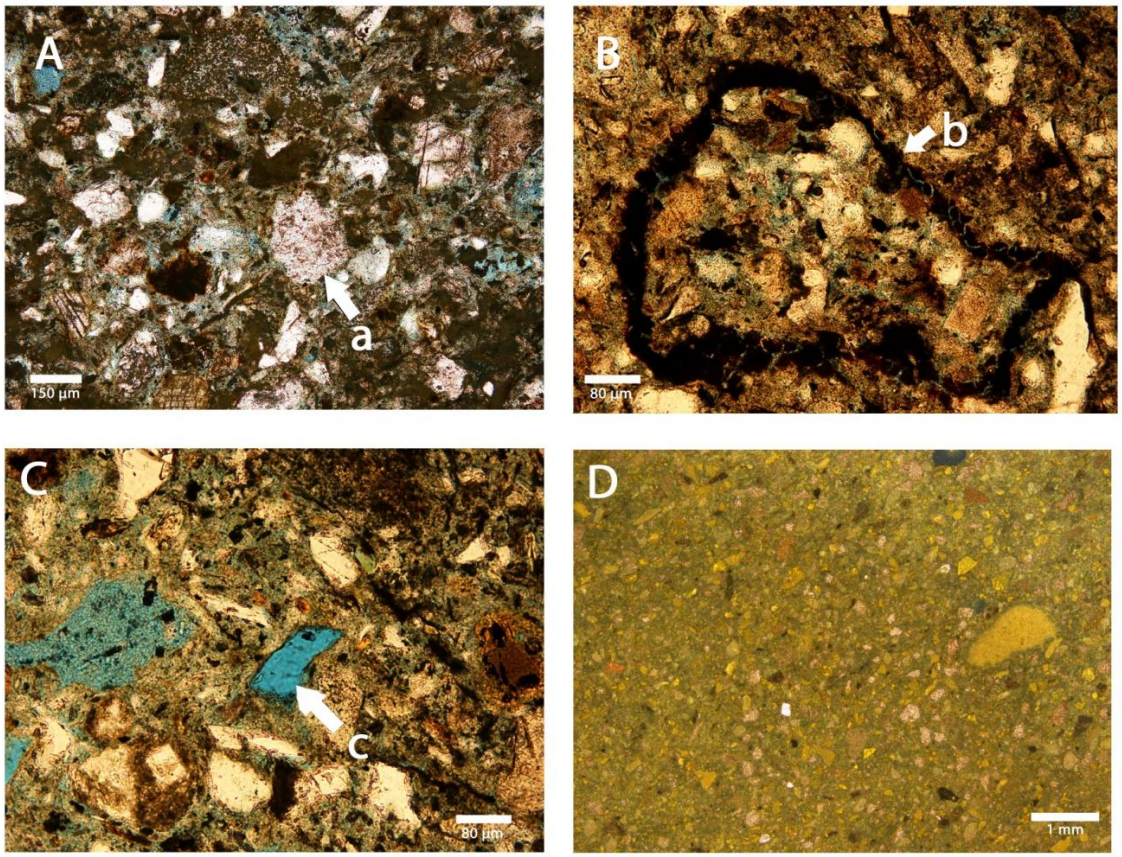


Figure 10. Photomicrographs of bone-bearing sandstone (A: 10x, scale bar = 150µm and PPL; B and C: 20x, scale bar = 80µm and PPL; D: 2x, scale bar = 1mm and PPL, stained with K-spar stain). Important features shown on figures included; a) feldspar grain altered to kaolinite; b) Fe-oxide outlining the original grain; c) complete grain dissolution. The yellow grains on D are stained by K-spar stain.

The stained section indicates high (up to 25%) feldspar content (Figure 10.D). Lithic fragments are also common (up to 30%) in the bone-bearing sandstone (Figure

10.D). Thus, the bone-bearing sandstone is a mud-rich feldspathic litharenite. Framework grains include quartz, feldspar, and volcanic rock fragments, and accessory minerals include calcite, Fe-oxide (hematite) and other mafic minerals. Feldspar and volcanic rock fragments often have an altered appearance (Figure 10.A-a). Grains are angular to subangular and grain contacts are point to almost floating. Fe-oxide sometimes outlines pre-existing volcanic rock fragments (Figure 10.B-b). Partial dissolution of grains is very common in the bone-bearing sandstone. Complete grain dissolution is also observed in bone-bearing sandstone (Figure 10.C-c), but is less frequent than in the basal sandstone.

Concretions

The spatial relationship between bone and concretion is summarized in the Figure 11. Concretions are present both inside and outside of the fossilized bones; these concretions exhibit similarities in terms of color, fabric, and enclosed grains regardless of where they form. Additionally, concretions formed on the rib and femur fragments do not exhibit significant difference in terms of color, fabric and enclosed grains. Petrographic analysis also indicates that grain inclusions increase toward the concretion-sandstone boundary (Figure 12).

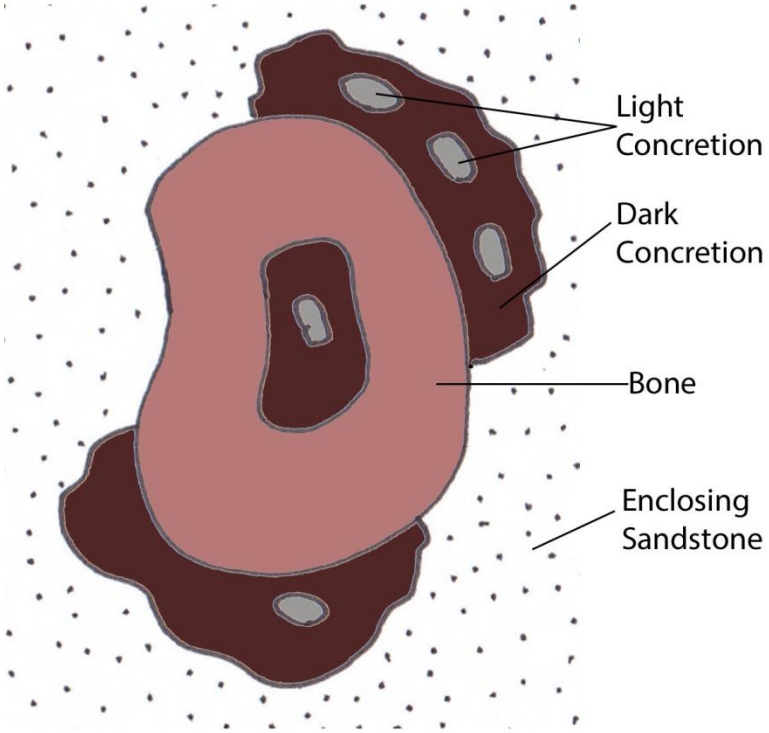


Figure 11. Schematic diagram of the spatial relationship among concretion, bone and sandstone. Concretions occur both inside and outside of fossilized bones. Concretions also consists two types of matrices; reddish brown and light gray matrices labeled light concretion and dark concretion respectively in the diagram.

Lighter matrices are gray in color and exhibit higher birefringence with polarized light whereas darker matrices are mostly opaque to red with single-polar light (with higher light intensity), suggesting the major mineral forming concretionary body is hematite. Concretions consist of two different colored matrices; light gray and reddish brown (Figure 13.A). Characteristics of the grains included in both matrices are the same; more angular and less altered compared to grains in the bone-bearing sandstone (outside of the concretion.)

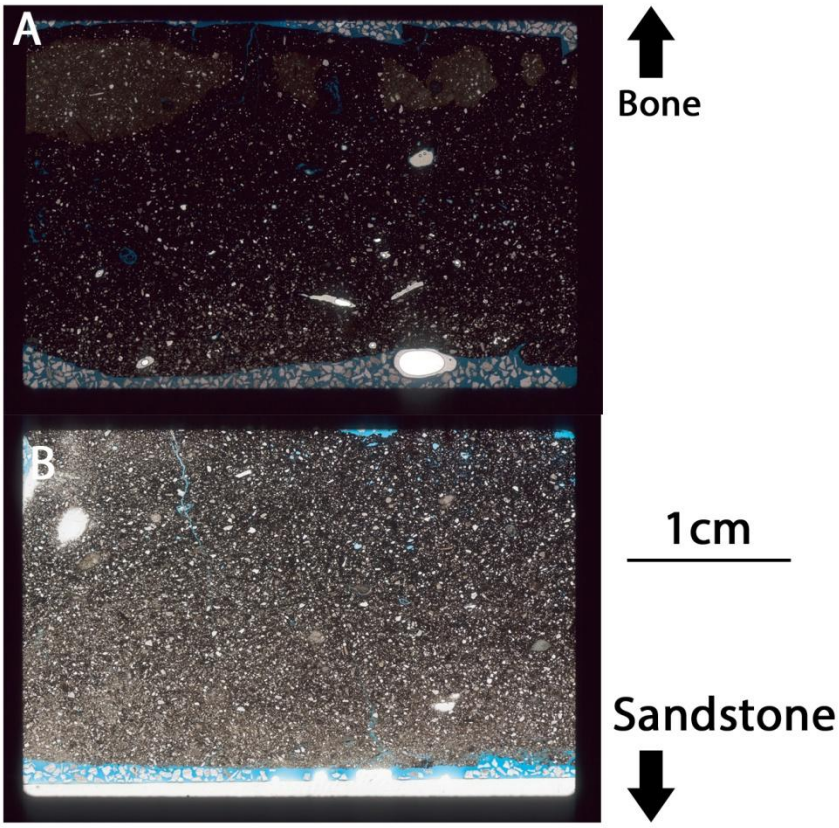


Figure 12. Two thin-sections of concretion formed on the humerus cut adjacent to each other. A) concretion in contact with bone. B) a part of concretion near the sandstone boundary. Grain contents gradually increase toward sandstone. Note: the color contrast is slightly off due to the camera setting; (A) is darker than (B).

Major grains enclosed are quartz, feldspar, calcite and volcanic rock fragments. The reddish brown and light gray matrices are referred as "dark" and "light" respectively, for the rest of thesis. The dark concretion is composed of hematite (Figure 13.B) and light concretion is composed of siderite. Many grains within the light colored matrices exhibit carbonate grain coatings (isopachous grain coating) (Figure 14.B-C) whereas such grain coating is absent in dark concretions (Figure 14.A). Some calcite grains are relatively large and resemble volcanic glass (Figure 14.D).

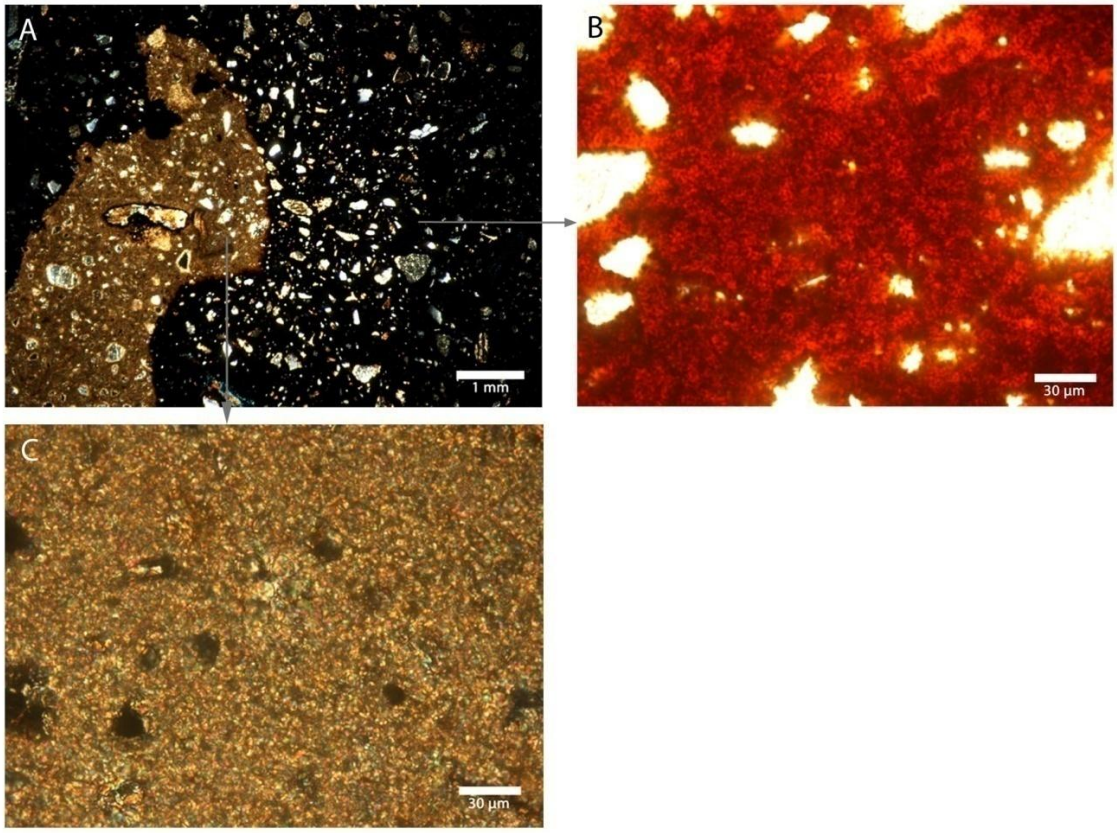


Figure 13. Photomicrographs of a concretion (A: 2x, scale bar = 1mm and XPL, B and C: 60x, scale bar = 30µm and XPL) showing different colored matrices. B) dark colored concretion exhibit bright red color with high light intensity suggesting dark concretion is composed of hematite; C) lighter colored matrices exhibit high birefringence with cross-polarized light suggesting the light concretion is composed of carbonate mineral.

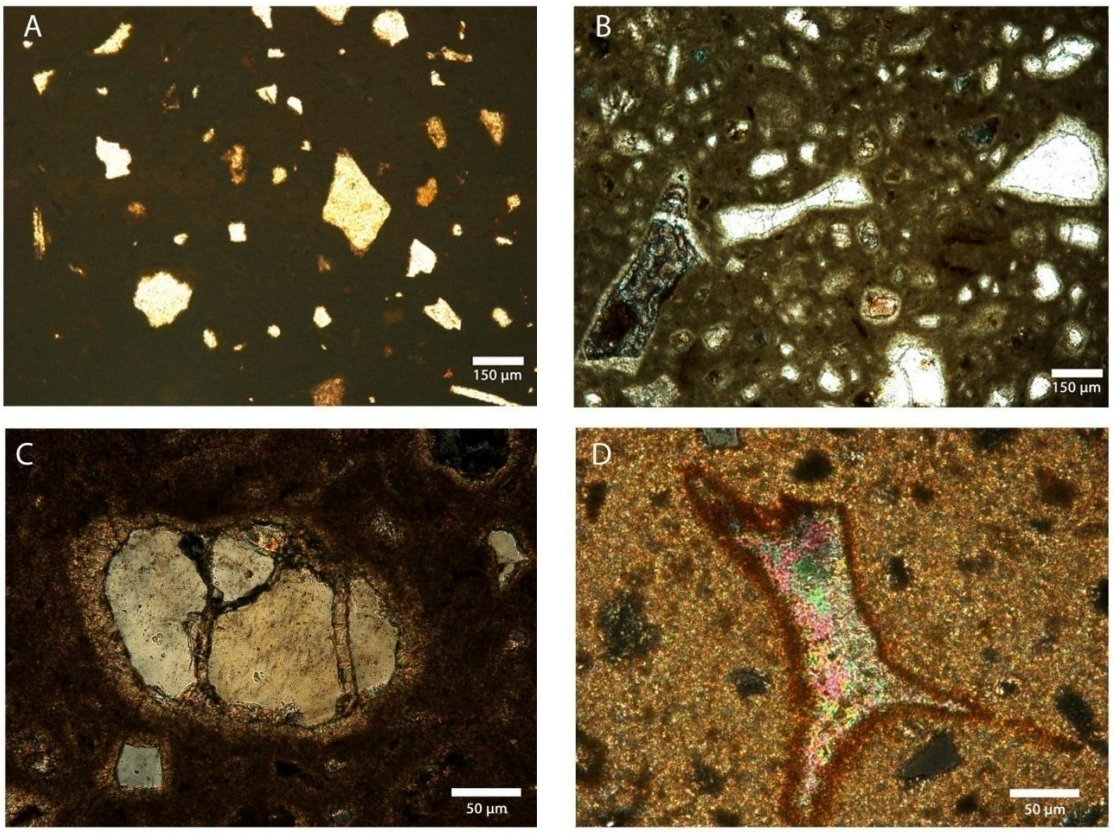


Figure 14. Photomicrographs of concretion (A and B: 10x, scale bar = 150µm and PPL; C and D: 40x, scale bar = 50µm and XPL). A) The grains in dark concretion lack grain coatings. B) The grains in light concretion exhibit grain coatings. C) A quartz grain in a light concretion showing grain coating with high birefringence. D) A calcite grain within a light concretion. The shape of the grain resembles volcanic glass, which in turn suggests that volcanic glass fragments were replaced by calcite.

Bones

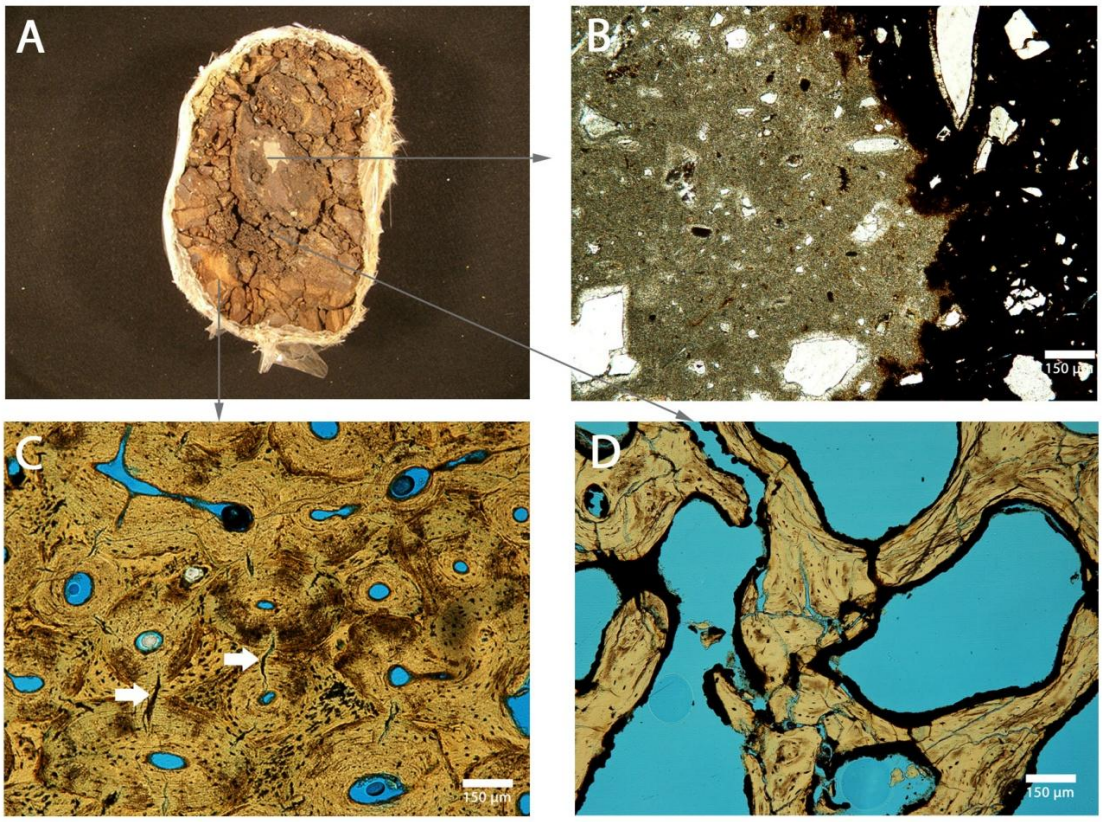


Figure 15. Fabric of femur and concretion; A) mesoscopic view of the femur (field of view is about 30cm); B) photomicrograph of concretion filling the marrow cavity exhibiting the similar characteristics to the concretion formed outside of the bone; C) photomicrograph of a cortex portion of the femur showing preserved microstructures; D) cancellous portion of the femur showing authigenic mineral precipitation in the voids. Photomicrographs B, C and D were taken with 10x, scale bar = 150µm and PPL. Arrows on C points at some of the radial fractures on the peripheral of osteon.

The marrow cavity of the femur is filled with a concretion similar to the concretion formed outside of the bone (Figure 15.A), containing similar grains, dark and light matrices and grain coatings in the light matrix (Figure 15.B). Concretion also fills

the cavity of rib. Both rib and femur samples include cortical (Figure 15.C) and cancellous bones (Figure 15.D).

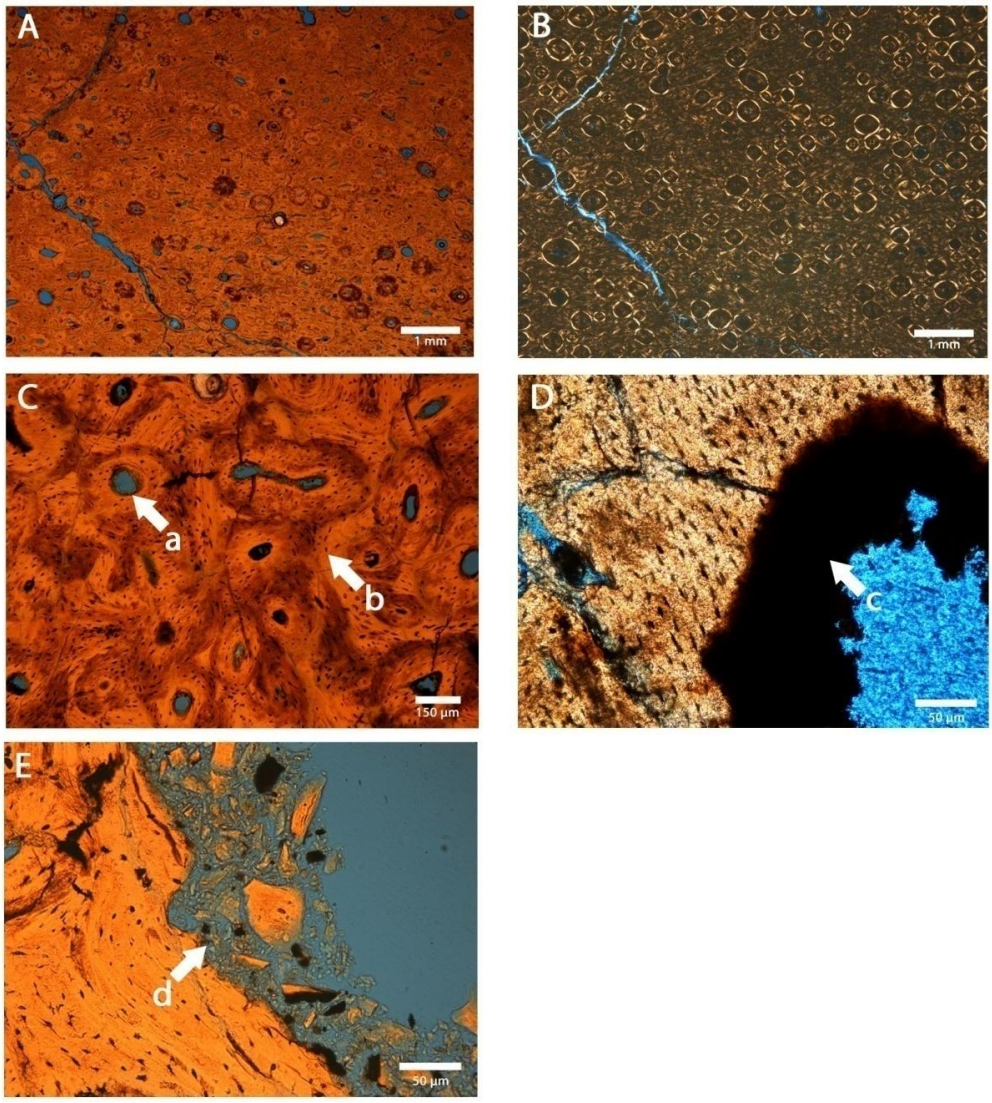


Figure 16. Photomicrographs of the femur (A: 2x, scale bar = 1mm and PPL; B: 2x, scale bar = 1mm and XPL; C: 10x, scale bar = 150µm and PPL; D and E: 40x, scale bar = 50µm and PPL). A and B show the same area, and preserved lamellae are easily observed with cross polarized light. C) The microstructures observed include; a) preserved Haversian canal and b) lacunae for osteocytes. D) A pore within cortical bone of the femur showing an opaque mineral precipitating inside Haversian canals (c). E) A larger pore in cancellous bone in the femur showing physical degradation of bone (d). Some fragments also show bone fragments are being altered to an opaque mineral. Note: The thin-section for D is not polished, which caused grainy texture on the micrograph.

Preserved bone microstructures include osteonal lamellae (Figure 16.A-B), Haversian canals (16.C-a) and lacunae for osteocytes (Figure 16.C-b). The radial cracks on the peripheral of secondary osteon (Figure 15.C) are indicative of expansion of collagen (Pfretzschner, 2006), and there are no fractures cross cutting these preserved microstructures. Smaller cavities in the cancellous bone and Haversian canals in the cortical bone remain mostly empty. However, these cavities exhibit evidence for authigenic mineral precipitation (Figure 16.D), physical degradation and alteration (Figure 16.E).

Cathodoluminescence

Cathodoluminescence is a phenomenon where a sample is bombarded by an electron beam and responding by emitting visible radiation (Marshall, 1988). Some impurity ions in minerals can serve as a centers for luminescence (activator) whereas other ions modify energy levels so that luminescence does not take place (quencher): for example, Mn^{2+} is a common activator and Fe^{2+}, Co^{2+} and Ni^{2+} are common quenchers in carbonate; Mn^{2+}, Ti^{4+} and Fe^{3+} produce yellowish green to blue luminescence whereas Fe^{2+} produce red luminescence in feldspar (Marshall, 1988). Thus, variation in the CL in the same mineral is indicative of different generations with different conditions of formation (Marshall, 1988).

Each rock sample exhibits an unique pattern of luminescence (Figure 15). The fossil samples did not lulminesce under CL.

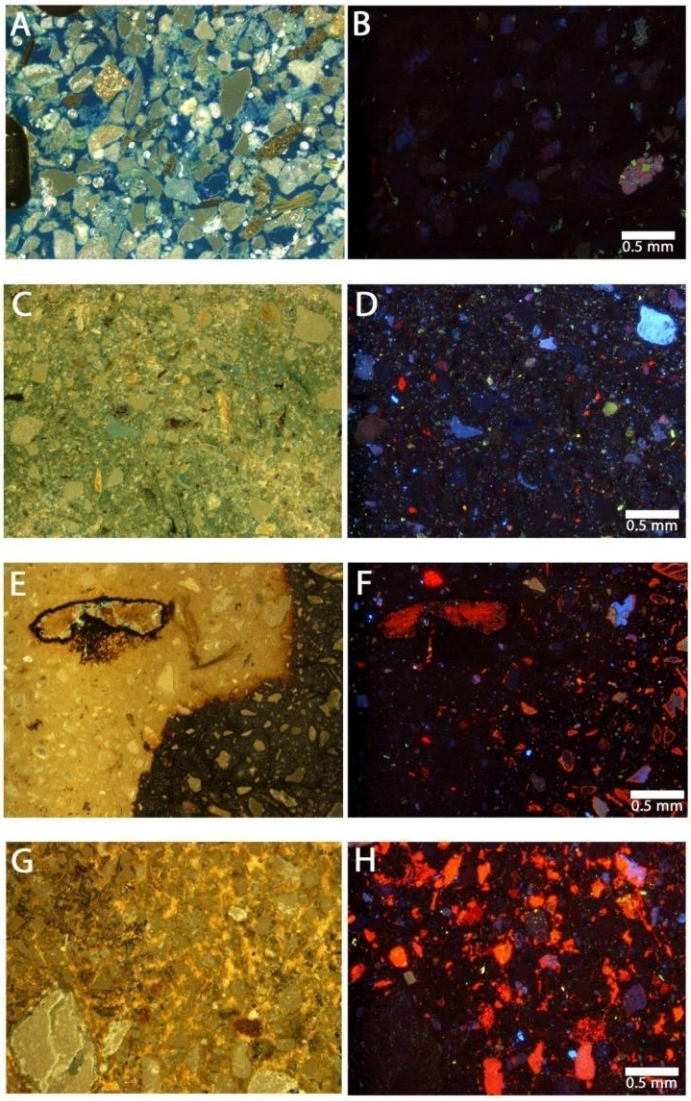


Figure 17. Photomicrographs (4x objective lens) with and without CL. A) Basal sandstone without CL. B) Basal sandstone with CL (98.5mTorr, 0.172mA, -8.8kV); luminescing grains include feldspar (blue and green) and volcanic rock fragment (pink). C) Bone-bearing sandstone without CL. D) Bone-bearing sandstone with CL; luminescing grains include feldspar (blue and green), calcite and/or dolomite (red) (95.0mTorr, 0.303mA, -8.8kV). E) Concretion near a fossil without CL; F) Concretion near a fossil with CL (95.5mTorr, 0.50mA, -8.8kV); luminescing grains include feldspar (blue), calcite and/or dolomite (red) and part of feldspar and volcanic rock fragments (red). G) Concretion near the concretion-sandstone boundary without CL; H) Concretion near the concretion-sandstone boundary with CL (91.0mTorr, 0.263mA, -8.8kV); luminescing grains include feldspar (blue), part of feldspar (red), and calcite filling cracks (red). Note: Quartz grains did not luminesce under CL; only some quartz grains had weak purple luminescence.

Basal Sandstone

Unlike other samples, bright red luminescence (such as for Fe^{3+} in feldspar and Mg^{2+} in calcite) was very rare in the basal sandstone (Figure 15.B). The blue luminescing grains are feldspar with Ti^{4+}. The pink to weak red signals on feldspar grains suggest feldspar grains are being altered to Fe^{3+} bearing mineral (e.g. clay). The yellowish green luminescence of potassium feldspar (Mn^{2+} impurity) is indicative of an igneous origin of euhedral grains.

Bone-bearing Sandstone

Various CL signals are observed in the bone bearing sandstone (Figure 15.D). Many bright red signals are observed; some crystals show rhombohedral crystal shape suggesting that they are either calcite or dolomite. Other red luminescing grains are likely volcanic rock fragments and feldspar with Fe^{3+} impurity based on crystal shape and altered appearance under non-polarized light. Large grains with blue luminescence are likely feldspar with Ti^{4+} impurity based characteristics observed with thin-section petrography (i.e. twinning). The matrix of the bone-bearing sandstone has numerous small luminescing areas, suggestive of microcrystalline feldspar and mafic minerals formed by alteration of feldspars and volcanic rock fragments (clay minerals do not luminesce with CL).

Concretion

The numerous small luminescent areas visible in the bone-bearing sandstone are absent in the concretion. Bright red CL signals are very common in the concretion and

are indicative of calcite, volcanic rock fragments, and feldspar grains. Distribution of the red signal varies slightly within the concretion; 1) lighter colored concretion, 2) darker colored concretion, and 3) near the sandstone/concretion boundary.

The lighter colored concretion tends to have more partially luminescent rims on the grains while fully luminescent rims on the grains are common in darker colored concretion (Figure 15.F). Additionally, many grain coatings within the light concretion do not luminesce with CL. Such grains sometime exhibit a partially luminescent rim. Conversely, many grains without grain coatings in the dark concretion exhibit a complete luminescent rim with CL.

More feldspar grains exhibit bright red luminescence toward the sandstone-concretion boundary (Figure 15.H). In comparison to dark colored concretion, alteration of feldspar grains is not limited near grain-matrix contact in sandstone-concretion boundary area. The carbonate cement filling cracks exhibits a red signal with CL. Such cement is found only in the sandstone-concretion boundary zone.

Scanning Electron Microscopy

Secondary electron imaging is used for morphology. Since heavy elements backscatter electrons more strongly than light elements, backscatter electron imaging (BSI) is used for phase discrimination.

Bone-Bearing Sandstone

The high Mg peak on the EDS spectrum suggests that the carbonate grains (bright red luminescence with CL) in the bone-bearing sandstone are dolomite (Figure 18.C).

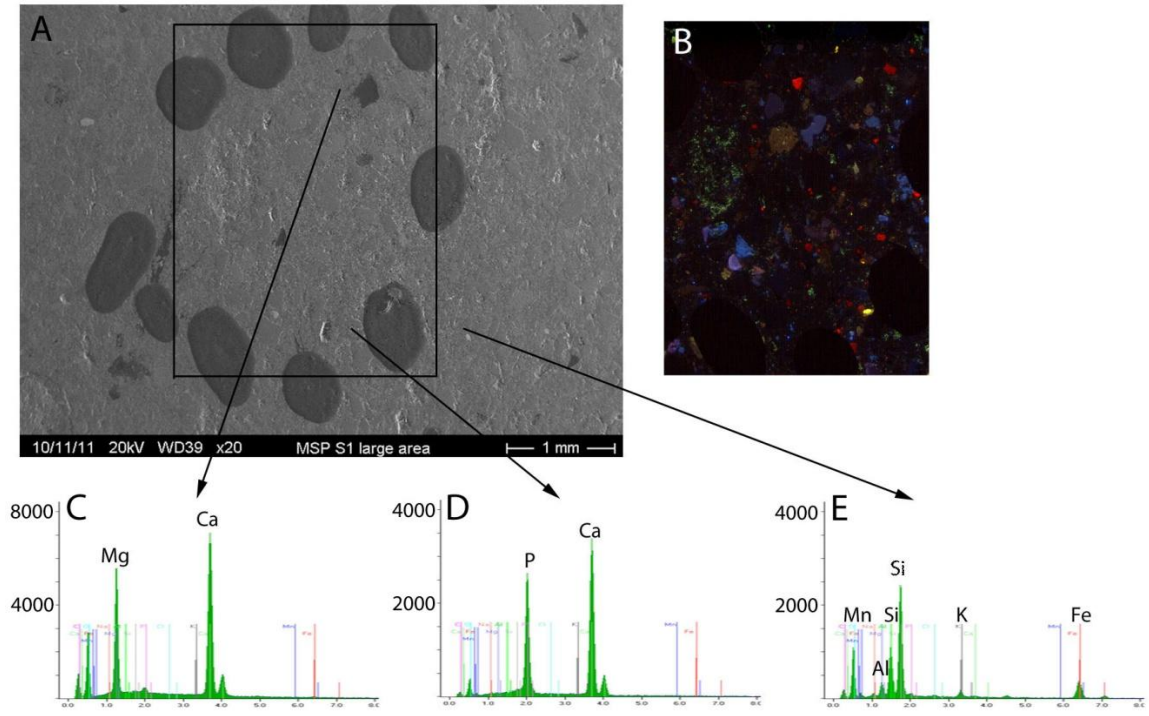


Figure 18. A) SEM micrograph of the bone-bearing sandstone. B) CL micrograph of the squared area as a reference. C) EDS spectrum indicating that the grain luminescing red with CL is dolomite. D) EDS spectrum indicating that the detrital grain luminescing bright yellow with CL is apatite; E) EDS spectrum of matrix including multiple mineral phases. Based on relatively high peaks of Si and Al, clay mineral is abundant in the sandstone matrix.

Another EDS spectrum suggests the grains that lumminesce bright yellow are detrital apatite (Figure 18.D). The EDS spectrum of the matrix suggests the sandstone matrix is mostly composed of clay minerals (Figure 18.E).

Concretion

The grain coatings in the light concretion exhibit different fabric in comparison to the matrices (Figure 19). However, such grain coatings do not exhibit significant differences in EDS spectra other than slightly higer peaks of Si and Al, suggesting that

the grain coating and matrix of the light concretion consist of the same mineral (i.e. siderite). Some quartz grains in the light concretion exhibit a partial red rim on CL micrographs (Figure 17.F, 19), and this partial rim is darker than the rest of grain coating in the SEM image (Figure 19) and matrix. The EDS spectra of the partial rim and the rest of the grain coating differ significantly: calcite versus iron bearing mineral (Figure 19.B-C).

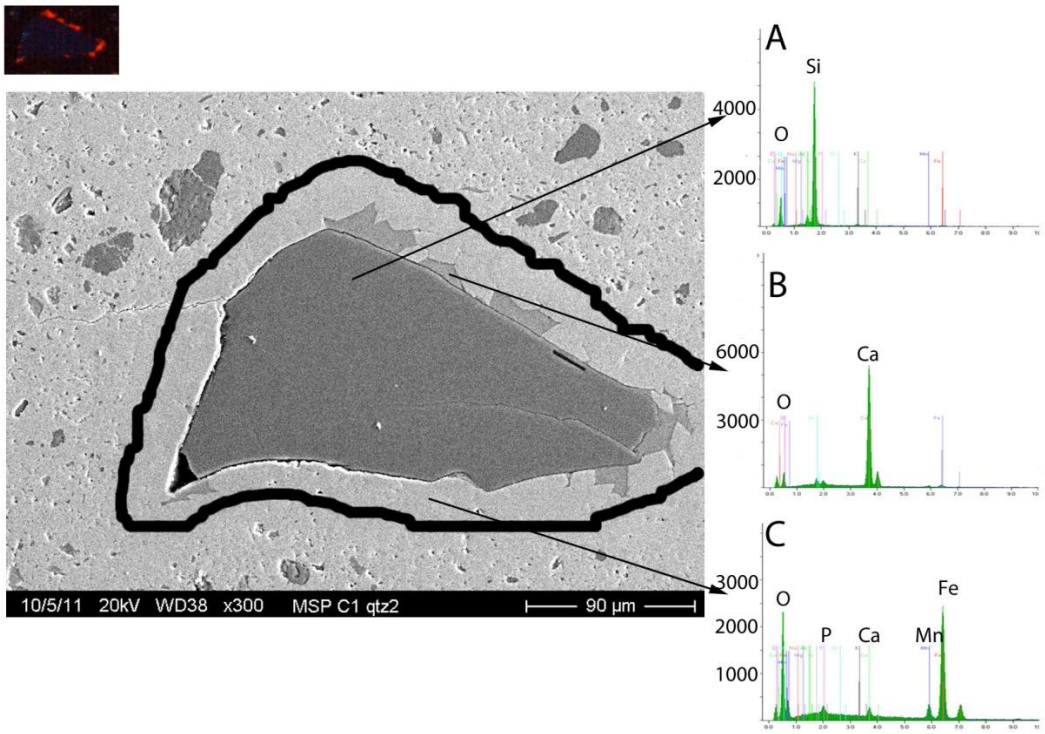


Figure 19. SEM micrograph of a quartz grain in light colored concretion showing partial rim of calcite. The black line outlines the entire grain coating (i.e. siderite). A) EDS spectrum of the quartz grain. B) EDS spectrum of calcite portion of the grain coating. C) EDS spectrum of the rest of grain coating. The high birefringence under petrographic microscope and high peak of iron on EDS spectrum suggest this mineral is siderite.

Many feldspar grains in the dark concretion exhibit complete bright red rims with CL (Figure 17.F, 21). The SEM micrograph also exhibits darker rim around feldspar

grains (Figrure 21). However, he EDS spectrum of such rim is almost identical to the matrix (i.e. siderite) (Figure 21.B-C).

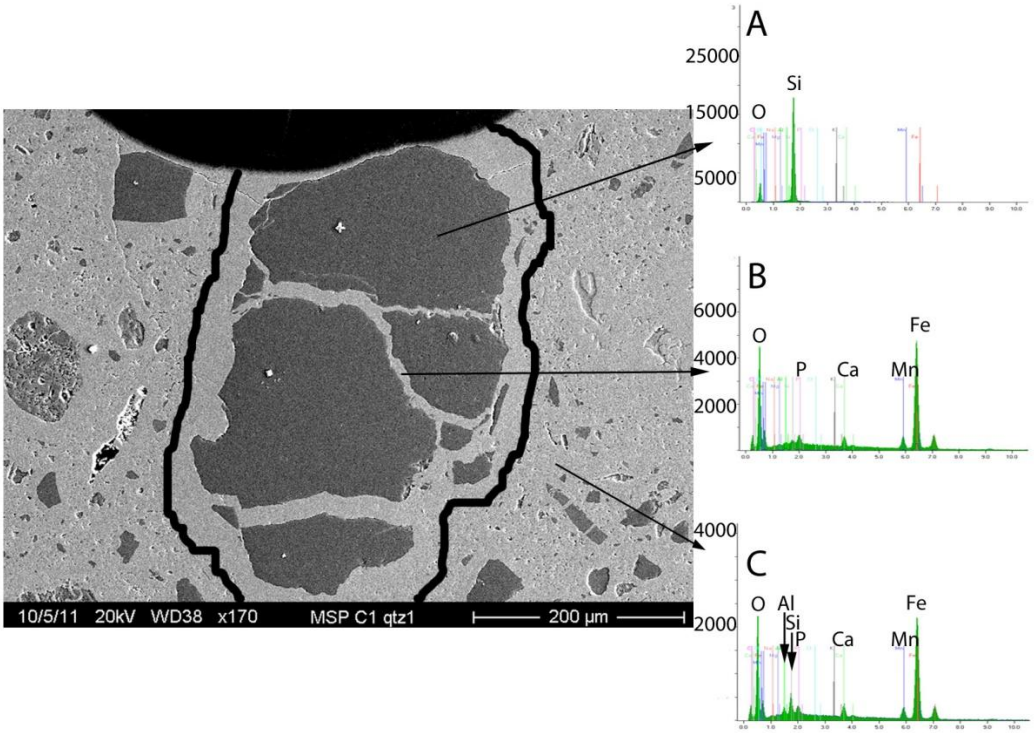


Figure 20. SEM micrograph of a fractured quartz grain in the light colored concretion. The black line outlines the grain coating. Black part on top of the micrograph is due to ink used for orienting the image under SEM. A) EDS spectrum of the quartz. B) Higher iron content and higher birefringence with petrography suggest this mineral is siderite. C) EDS spectrum of the matrix suggesting that siderite is main constituent of the matrix. The presence of Al and Si peaks indicates that this spectrum includes multiple mineral phases such as clay minerals. Note: A photomicrograph of the same grain is shown in Figure 8C.

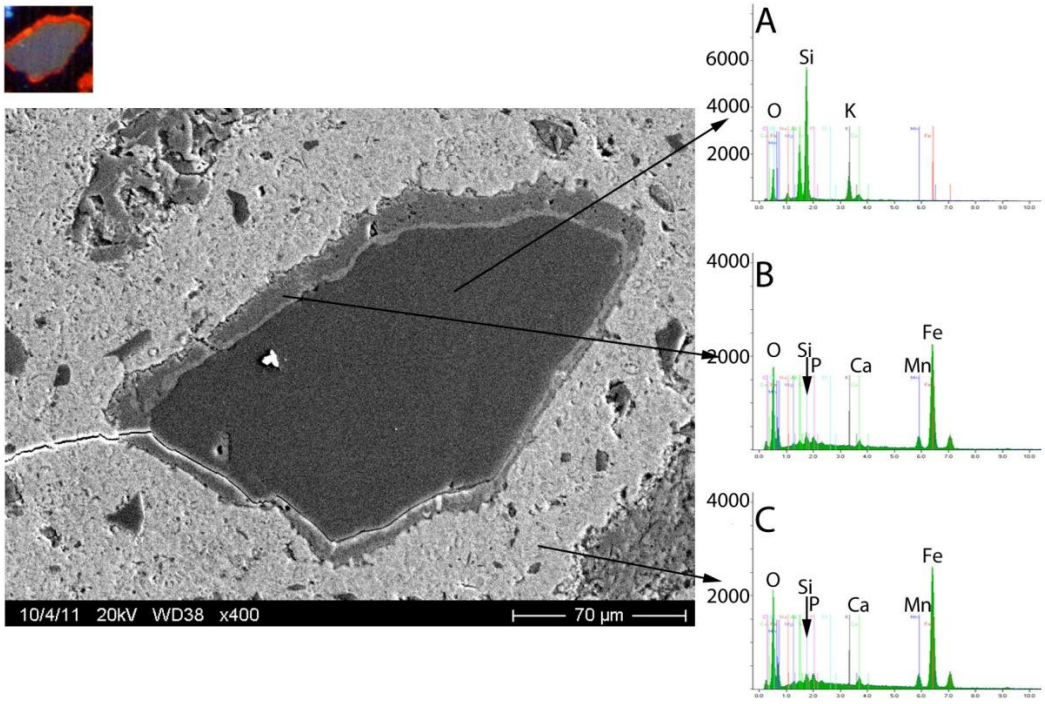


Figure 21. A SEM micrograph of feldspar grain with darker rim in dark concretion. A) EDS spectrum of the feldspar grain. B) EDS spectrum of the rim indicating that hematite is main constituent of this rim. C) EDS spectrum of the dark concretion matrix indicative of hematite. Si and P peaks in B and C may indicate the EDS spectra contains more than one mineral phases.

Bones

The lamellae of the Haversian system observed petrographically are not visible in the secondary electron image. However, a backscattered electron image captures such fabric (Figure 23.A). An SEM micrograph of the Haversian canal indicates coatings on inner wall contain three different material phases; fine grained minerals, lithic fragments and bright mineral (Figure 22). An EDS spectrum of the bright mineral contains the prominent barium peaks (Figure 22.A), suggesting that the bright mineral is barite. An EDS spectrum of the lithic fragment indicates it is a quartz grain (Figure 22.B). An EDS

spectrum of the finer grain is identical to the spectrum of fossilized bone mineral (Figure 22.C), suggesting bone is physically degrading.

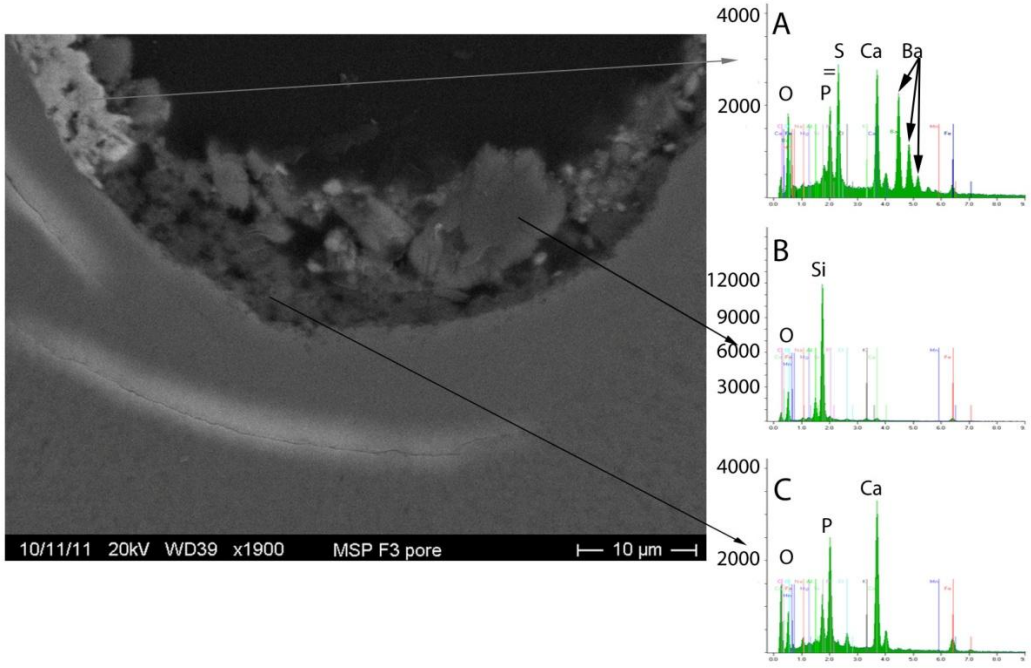


Figure 22. SEM micrograph of Haversian canal showing three distinctive materials filling the pore space. A) EDS spectrum of the brighter colored mineral in the SEM image. Prominent peaks of Ba and S indicates barite is present. Presence of Ca and P indicates that this spectrum is derived from multiple mineral phases (i.e. barite and apatite). B) EDS spectrum of lithic fragment filling pore space in a fossil bone. High peaks of Si and O indicates quartz. C) EDS spectrum of fine grained mineral adjacent to the bone suggesting such fine grained mineral is degrading bone fragment (apatite).

Electron mapping indicates that silica and barium are concentrated around the edges of pores (Figure 23.B). Sulfur is often associated with barium instead of iron, suggesting sulfur is present as barite instead of pyrite. Sulfur is also present within bone matrix without association with barium (Figure 23.C). Calcium, phosphorous and fluorine are always in close association, suggesting they are mainly present as fluorine-bearing apatite in the bone matrix (Figure 23.D).

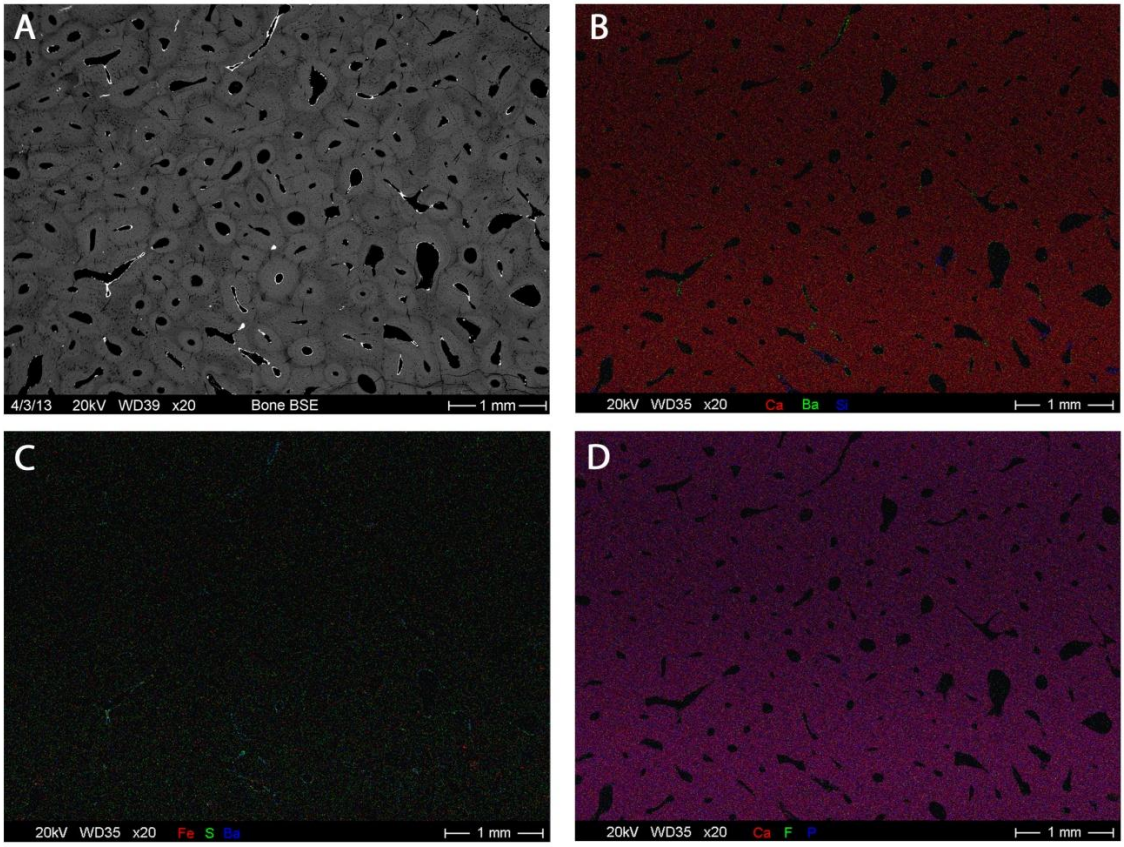


Figure 23. Backscattered electron micrograph and elemental mapping. A) Backscattered electron image as a reference. B) Calcium (red), barium (green) and silicon (blue); showing barium and silicon are concentrated in the pores. C) Iron (red), sulfur (green) and barium (blue); sulfer is concentrated in the pores, but also present within bone matrix. D) Calcium (red), fluorine (green), and phosphorous (blue); these three elements occur mainly in the bone matrix.

X-Ray Diffractometry

XRD was used for surveying for mineral identification in bulk samples and clay mineral analysis.

Full Range (10-70°) Scan

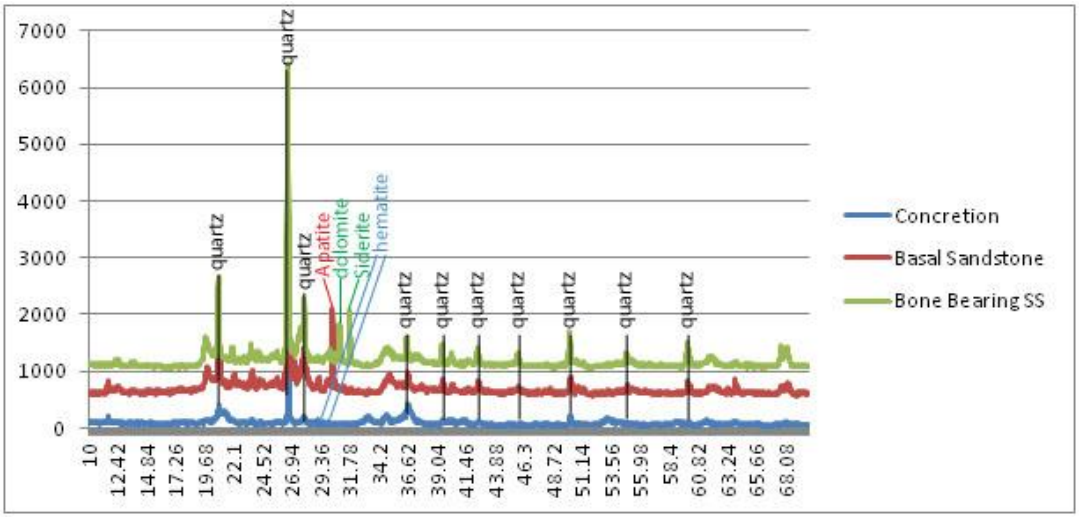


Figure 24. XRD spectra of random mount samples including concretion, basal sandstone and bone-bearing sandstone. Quartz is present in all samples. Apatite is unique in the basal sandstone. Dolomite and siderite are unique to the bone-bearing sandstone, and hematite is unique to the concretion. Black lines and labels indicates common appearance of the peak.

The quartz peaks are very prominent and feldspar peaks are also present between two prominent quartz peaks around 27°(2θ) in all the rock samples. Each rock sample includes unique peaks around 28-35°(2θ); one peak around 30°(2θ) for the basal sandstone, two peaks around 29-32°(2θ) for the bone-bearing sandstone, and two peaks around 34-36°(2θ).

Basal Sandstone. XRD spectra demonstrate that apatite is present in the basal sandstone. The known spectrum of apatite (211) matches with the sharp peak at around 30-31°(2θ) and other small peaks of the basal sandstone spectrum. The XRD spectrum of the basal sandstone also includes a peak around 27-28°(2θ) suggesting the presence of biotite. This peak is absent in concretion and bone-bearing sandstone spectra.

Bone-bearing Sandstone. One sharp peak at around 32°(2θ) matches up with a known spectrum of siderite ((104) peak), and the other peak at around 29°(2θ) matches up with a known spectrum of dolomite ((104) peak) (Mindat). Calcite peaks were not present in the bone-bearing sandstone.

Concretion. Two unique peaks on the concretion spectrum at around 33-35°(2θ) range match with a known spectrum of hematite ((104) and (110) peaks) (Mindat), which coincides with result from petrography. Although hematite seems to be the main constituent of the concretionary body based on petrography, the peaks for hematite are much lower than those for quartz. The siderite peaks were absent in the XRD spectrum of concretion.

Bone. Cortical and cancellous bone show almost identical XRD spectra (Figure 25).

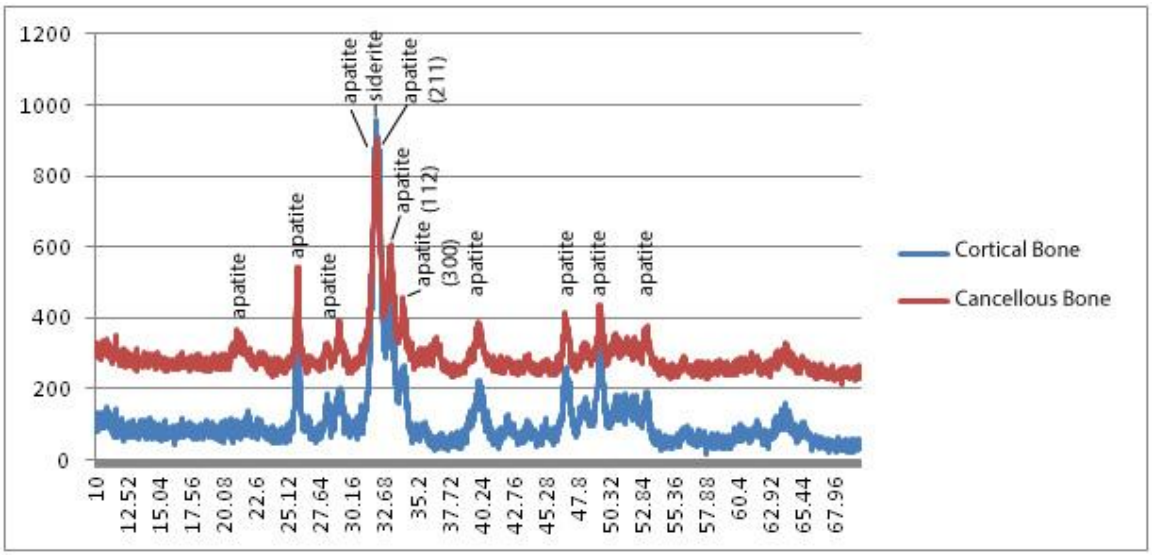


Figure 25. XRD spectra of cortex and cancellous bones showing no significant difference. The major peaks are apatite. Siderite is also present in the fossil bone.

Many significant peaks match with the peaks of the known hydroxyl- and fluor-apatite spectra. The sharp peak at around 32°(2θ) suggests presence of siderite within the bone matrix. Another sharp peak at around 32°(2θ) is likely dolomite. Even though hematite commonly fills the cavity, XRD spectra of the fossilized bone do not include the hematite peaks.

Clay Mineral Analysis

Basal Sandstone. The XRD spectra of the basal sandstone within clay range (3-28°(2θ)) indicate that the clay minerals included in the basal sandstone are illite, montmorillonite, kaolinite and interstratified montmorillonite-illite (Figure 26).

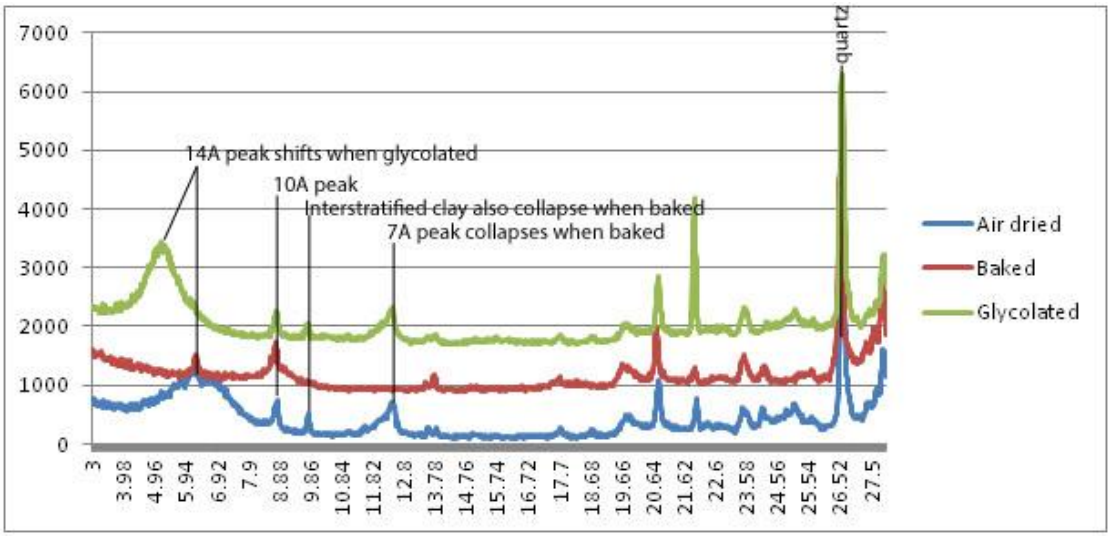


Figure 26. XRD spectra of the basal sandstone. Three treatments following protocols from Moore and Reynolds (1997) are shown in different color. 7Å peak collapses when baked, indicating kaolinite is present. 10Å peak do not collapse or expand with treatments, indicating illite is present. 14Å peak shifts when glycolated, indicating montmorillonite is present. Interstratified montmorillonite-illite peak is present at around 10°(2θ).

The 14Å peak in the air-dried sample decreases intensity when baked and shifts to 17Å when glycolated, suggesting the presence of montmorillonite. The 10Å peak does not shift or disappear when baked or glycolated, suggesting the presence of illite. The 7Å peak disappears when baked, which may suggest the presence of kaolinite or chlorite. Since the 14Å peak only partially collapses when baked, and a broad peak on the glycolated spectrum around 17Å may include 14Å range, both chlorite and kaolinite are likely present in the basal sandstone. There is a unique peak around 9Å in the air-dried spectrum. This peak disappears when baked and does not change when glycolated, suggesting interstratified montmorillonite-illite is also present.

Bone-bearing Sandstone. Comparison of XRD spectra of three oriented samples from the basal sandstone within the clay range (3-28°(2θ)) indicates clay minerals present in the bone-bearing sandstone are illite, montmorillonite, and kaolinite (Figure 27). The 14Å peak in the air-dried sample disappears when baked and shifts to 17Å when glycolated, suggesting the presence of montmorillonite. The 10Å peak does not shift or disappear when baked or glycolated, suggesting the presence of illite. The 7Å peak disappears when baked, which may suggest the presence of kaolinite or chlorite. Since the 14Å peak collapses when baked, chlorite is less likely to be present. Thus, kaolinite is present in the basal sandstone instead of chlorite. The interstratified montmorillonite-illite is absent in the bone-bearing sandstone.

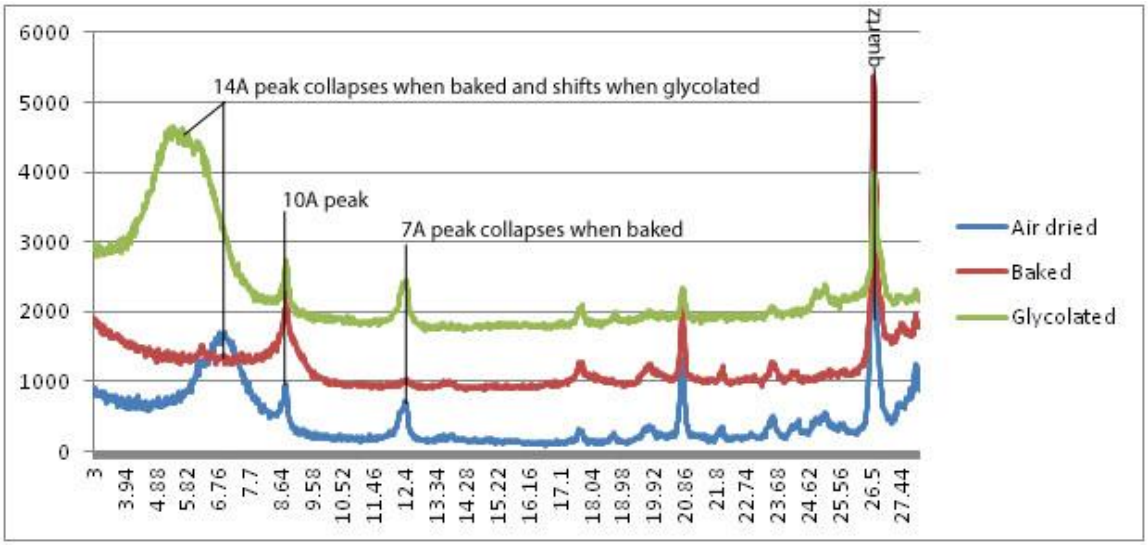


Figure 27. XRD spectra of bone bearing sandstone. Three treatments following protocols from Moore and Reynolds (1997) are shown in different color. 7Å peak collapses when baked, indicating kaolinite is present. 10Å peak do not collapse or expand with treatments, indicating illite is present. 14Å peak shifts when glycolated, indicating montmorillonite is present.

Concretion. The XRD spectra from the concretion show less prominent peaks in comparison to the other samples. However, air dried spectra show 10Å and 7Å peaks suggesting presence of illite and a kaolinite group clay, respectively (Figure 28). The 7Å peak disappears when baked and glycolated. Halloysite is a 7Å clay which expands when glycolated; however, halloysite occurs due to hydrothermal alteration (Mindat). Thus, identification of 7Å clay mineral may need further investigation. The 10Å peak does not change when baked and glycolated suggesting illite is present. The 14Å range in air dried spectrum shows broad peak and the baked spectrum also show a small peak around 14Å range. Additionally, the glycolated spectrum has a peak at around 17Å. Although the 14Å is not clear in the air-dried spectrum, this may suggest the presence of montmorillonite.

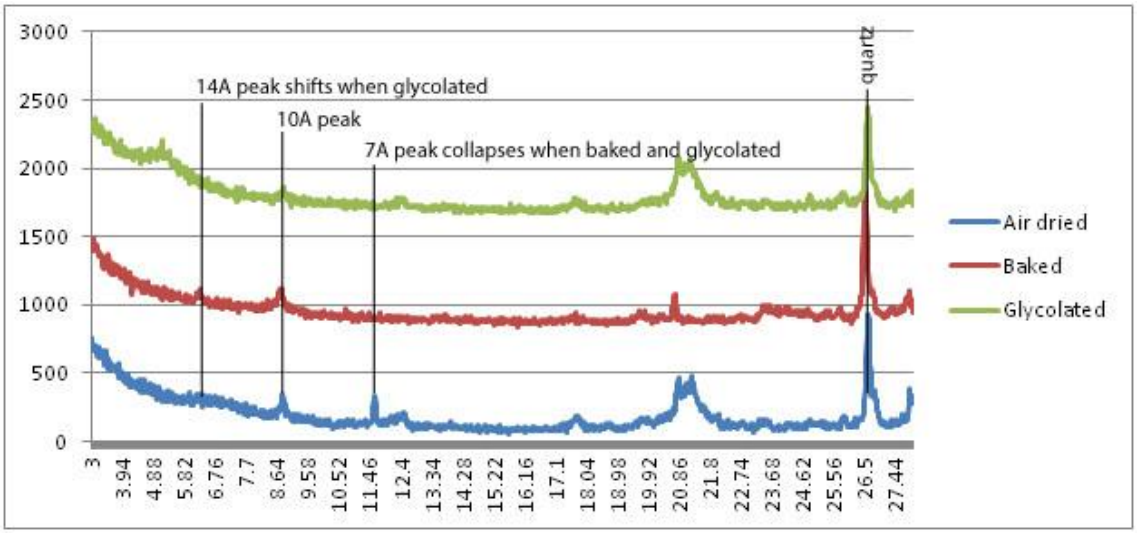


Figure 28. XRD spectra of concretion. Three treatments following protocols from Moore and Reynolds (1997) are shown in different color. Relatively lower peaks are indicative of lower clay content than sandstone samples. 7Å peak dissapears when baked and glycolated, suggesting kaolinite or halloysite is present. 10Å peak does not shift or collapse, suggesting . 14Å peak shifts when glycolated suggesting montmorillonite is present.

DISCUSSION

Taphonomy

Weathering of bone ranges from stages 1-3 (Table 2) suggesting some bones in the bone assemblage were exposed to the surface for up to 15 years (Behrensmeyer, 1978). Such a temporal window exposes skeletal remains to destructive biological activities such as scavenging and stomping by larger animals. A bone fragment found in this assemblage exhibiting the possible bite mark suggests the possible presence of scavengers. In order to support such an interpretation, more fossils need to be collected and the dimension of the possible bite marks analyzed.

The gray mud and poorly developed paleosol in the bone-bearing sandstone is indicative of a poorly drained depositional setting. Homogenized massive texture in the bone-bearing sandstone is likely due to the bioturbation by plant roots and animals. Such biological activity can also destroy bones; e.g. plant roots tend to destroy bones to acquire phosphorous. Thus, biological activities both on the surface and in soil could cause non-selective destructions of bones, which explains the absence of articulated skeleton and sorting in the bone-bearing sandstone.

Sorting and Orientation

The fossil assemblage does not exhibit any sorting in terms of the skeletal element or size, suggesting that biological and mechanical sorting did not take place at the time of deposition. The depositional environment is interpreted as a crevasse splay, a low energy depositional environment associated with crevassing events. The fossils in this

assemblage exhibit minimal abrasion (stages 0-1) and do not exhibit any sorting (i.e. hydraulic sorting discussed in Voorhies, 1969). These are also indicative of a low energy depositional setting. Thus, taphonomic data support with the interpreted depositional environment.

The larger fossils show no preferred orientation. However, the sample size of skeletal remains in the assemblage is not large enough to conduct any statistical analysis; thus such interpretation is only suggestive.

Bone Modification

The abrasion is consistently low, which suggests the depositional environment was a low energy setting. However, the mode of breakage is variable regardless of the size, suggesting the introduction of the skeletal remain to the depositional system is variable. For example, the bones from in situ fauna experience minimal transportation, whereas bones can also be introduced from the channel breaching the levee. Thus, the assemblage is also time-averaged.

Diagenesis

Diagenetic Processes Recorded

Basal Sandstone. The diagenetic processes recorded in the basal sandstone include: 1) early precipitation of calcite, 2) clay mineral precipitation prior to grain dissolution, 3) physical compaction, 4) alteration and dissolution of grains, 5) clay authigenesis and 6) carbonate precipitation during late diagenesis.

Early precipitation of calcite is evidenced by the exploded fabric of biotite (Figure 11.B-d). Such displacive overgrowth of calcite is indicative of the calcite precipitation in the vadose zone (Braithwaite, 1989). The calcite cements were dissolved by further diagenesis in the basal sandstone, leaving secondary pores between biotite crystals.

Clay mineral precipitation prior to grain dissolution is evidenced by the oversized pores outlined by clay minerals in the basal sandstone (Figure 11.A-b). Alteration of feldspar during early diagenesis (diagenetic temperature of <25°C) produces kaolinite (Wilson and Pittman, 1977; Boggs, 2003, pp.401-404). Presence of kaolinite is evidenced by XRD data (Figure 26), hence early kaolinite precipitation is supported by multiple lines of evidence.

Overgrowth of quartz is indicative of physical compaction; burial depth of 1 to 1.5km and temperature of 55°-75°C (Dutton and Diggs, 1990). However, overgrowth of quartz can be inherited from provenance, hence it is only suggestive. Physical compaction of basal sandstone is also supported by bent mica and ductile grain deformation (Figure 9.B).

Skeletonized grains of feldspar and oversized pores (Figure 9.A) are indicative of grain alteration and dissolution. As previously mentioned, feldspar alters to kaolinite during early diagenesis (<25°C). Such processes could also occur during uplift (i.e. telogenesis). Additionally, complete grain dissolution is likely indicative of accelerated diagenesis at a deeper diagenetic stage (i.e. mesogenesis). Thus, alteration and dissolution of grains took place in various stages of diagenesis.

Interlaminated illite-montmorillonite is unique to the basal sandstone and interpreted as a product of clay authigenesis at high temperature (>55°C). Montmorillonite is a product of volcanic rock (e.g. volcanic glass) degradation, and such reaction take place during eogenesis and mesogenesis (Boggs, 2003, p. 402). Two clay authigenesis reactions suggested by Boles and Franks (1979) include:

Reaction 1

$$4.5K^{+} + 8Al^{3+} + \text{smectite} \rightarrow \text{illite} + Na^{+} + 2Ca^{2+} + 2.5Fe^{3+} + 2Mg^{2+}\ 3Si^{4+} + 10H_2O$$

and

Reaction 2

$$3.93K^{+} + 1.57\text{smectite} \rightarrow \text{illite} + 1.57Na^{+} + 3.14Ca^{2+} + 4.28Mg^{2+} + 4.78Fe^{3+} + 24.66Si^{4+} + 57O^{2-} + 11.40OH^{-} + 15.7H_2O$$

These reactions suggest that mesogenetic pore-fluid in the basal sandstone was rich in K^{+} ions.

Since freshly broken surfaces of the spheroidal concretions react with weak acid, these concretions are likely indicative of carbonate precipitation after uplift (i.e. telogenesis). Such an interpretation is supported by lack of carbonate cementation elsewhere in the basal sandstone; petrography, CL, and XRD did not detect any carbonate mineral. These concretions are well cemented sandstone, which differ from concretions found in the bone-bearing sandstone. These spheroidal concretions may contain a unique set of diagenetic information, however, they were not analyzed in this study.

Bone-Bearing Sandstone. The diagenetic processes recorded in the bone-bearing sandstone and enclosed concretion include: 1) calcite precipitation in the vadose and/or zone, 2) siderite precipitation in the phreatic zone and/or alteration of calcite to siderite, 3) formation of siderite concretions, 4) oxidation of siderite concretions, 5) grain alteration and dissolution, 6) dolomite precipitation after grain dissolution.

Two mineral phases are found in the grain coatings preserved in concretion; siderite and calcite (Figure 18). Such differences in mineral phase suggest different geochemistry of the pore-fluid they precipitated from; hence the two mineral phases precipitated from different diagenetic fluid. Alternatively, they could precipitate from the in the same diagenetic fluid with gradual loss of Ca^{2+}, which in turn cause siderite to precipitate instead of calcite. Additionally, meniscus and pendant grain coatings are indicative of vadose cementation whereas isopachous and blocky fabrics are indicative of phreatic cementation (James and Choquette, 1983). Since vadose grain coatings exhibit partial rims in the thin-section, the calcite portion of the grain coating is interpreted as vadose origin. Isopachous fabric is observed in the majority of grain coatings (Figure 14.B), hence siderite precipitated in the phreatic zone.

The concretions forming on outer surface and within marrow cavities of fossil bones are mostly hematite (Figures 13 and 15). Curtis and Coleman (1986) states that iron oxides and hydrated iron oxides are most probably secondary oxidation products when seen in ancient concretions. These concretions include smaller siderite matrices, suggesting concretionary bodies were originally composed of siderite and oxidized during subsequent diagenesis. Since these concretions include phreatic grain coatings,

concretion precipitation must have taken place in the phreatic zone (after grain coating) or later during mesogenesis or telogenesis.

The high clay content in the bone-bearing sandstone makes it difficult to distinguish primary and secondary pores as well as generation of authigenic clay minerals. Some pores exhibit the shape of pre-existing grains, suggesting grain dissolution took place in the bone-bearing sandstone. As discussed in the previous section, alteration of feldspar is accelerated in deeper burial (i.e. mesogenesis). Thus, such grain dissolution is likely indicative of deeper burial (i.e. mesogenesis).

Unlike the basal sandstone, carbonate cements are present in the bone-bearing sandstone matrices as indicated by CL micrographs (Figures 17.D and H). Bright red luminescence under CL suggest these carbonate cements are either calcite or dolomite. Several carbonate cements analyzed with EDS included high Mg peaks (not provided in the results section) suggesting the carbonate cements are high-magnesian calcite or dolomite. Additionally, carbonate cements are especially common near the sandstone - concretion boundaries, suggesting concretions may provide ions for carbonate precipitation (i.e. Ca^{2+} and Mg^{2+}) or act as nucleation sites for carbonate precipitation.

The interlaminated illite-montmorillonite found in the basal sandstone is absent in the bone-bearing sandstone and concretion. The diagenetic temperature in the both sandstones are comparable; 7m stratigraphic separation with a geothermal gradient of 2.7°C/100m (Schmidt and McDonald, 1979) produce temperature difference of only 0.19°C; hence lack of interlaminated clay is indicative of different pore-fluid

geochemistry. Clay authigenesis requires K^+, suggesting the bone-bearing sandstone pore-fluid at deeper burial was depleted in K^+.

Fossil Bones. The diagenetic processes recorded in the fossil bones include: 1) alteration of bone apatite with close temporal association with collagen degradation, 2) infiltration by pore-fluid, 3) precipitation of barite, 4) permineralization by siderite, and 5) further alteration of bone apatite.

The fossil bones preserve bone microstructures (Figures 15 and 16). This is likely due to the preserved fabric of the bone mineral (i.e. orientation of apatite crystallites c-axes), which require seeded overgrowth of bone apatite (Hubert et al., 1996; Trueman and Tuross, 2002). Due to its extremely small crystal size (350-400Å x 350-400Å x 25-50Å (Weiner and Price, 1986)), bone mineral is highly reactive (Trueman and Tuross, 2002). Thus, exposure of bone minerals by quick collagen degradation likely leads to complete dissolution of bones. Since collagen in bone can be removed both by microbial activity and hydrolysis (e.g. Pfretzschner, 2006), limiting such reaction may be essential for bone preservation. Dehydration of collagen restricts hydrolysis, and also rehydration of dehydrated collagen introduces ions for permineralization and authigenic mineral precipitation (Lingham-Soliar and Glab, 2010). Thus, dehydration of collagen is likely one of the contributing factors for the preservation of the bone studied.

Polygonal fractures crosscutting the microstructures are indicative of deformation at deeper burial levels (Pfretzschner, 2000). Such fractures are uncommon in the fossil bones, suggesting mechanical effect of compaction of the bone-bearing sandstone is minimal. Radial fractures peripheral to the osteon (Figure 15.C) are indicative of

collagen hydration rather than compaction (Pfretzschner, 2006; Pfretzschner and Tuken, 2011). Thus, the bone experienced minimal compaction at deep burial levels.

Infiltration by pore-fluids is evidenced by the presence of lithic fragments in Haversian canals (Figure 22). This suggests pore-fluid for fossilization of the bones was not separated from the lithification of the sandstone. However, pores in the fossil bones contains an unique authigenic mineral, barite. The possible explanation is that collagen degradation in early diagenesis locally provided sulfur for barite precipitation. However, barite can precipitate under various pore-fluid geochemistry conditions (Wings, 2004), making interpreting of such a reaction cause difficult.

Petrographic analysis (Figure 16.E) indicates the physical degradation of fossil bone minerals is evidenced by fraking of the inner surface of Haversian canals and alteration of such fragment to opaque minerals (possibly clay or iron oxide). This suggests that fossil bone mineral is metastable under surface conditions. Since fossil bones presumably experienced increase temperature and pressure conditions during burial, it is interpreted that fossil bone minerals were altered to the more stable mineral at higher temperature and pressure.

Mechanical Effect of Compaction

Fossil bones often exhibit plastic deformation, and such deformed bones exhibit polygonal fractures crosscutting original microstructures in microscopic scale (e.g. Pfretzschner, 2000; Gonzalez Riga and Astini, 2007). Although the sandstones exhibit evidence for mechanical compaction (i.e. bent mica, ductile grain deformation), the fossil bones studied do not exhibit significant deformation due to compaction at either

mesoscopic or microscopic scales (Figure 15 and 16). This suggests two possible scenarios: 1) the lithostatic pressure was not high enough to cause deformation in fossil bones; and 2) diagenetic effects such as permineralization and bone mineral alteration minimized the effect of mechanical compaction.

In order to test these hypotheses, burial depth needs to be estimated as well as analyzing the grains and fabric of the sandstone. Deformed grains such as bent mica and ductile grain deformation provide qualitative evidence of mechanical compaction of sandstone (Boggs, 2003, p. 359); hence presence of such grains suggest that these sandstones experienced deep burial during diagenesis. Primary pore analysis is also utilized for estimating burial depth; such analysis include differentiating from secondary pores such as partial and complete grain dissolution/alteration, presence of molds, pores within grains, and fractured grains (Boggs, 2003, p. 359). Secondary pores are common in both sandstones. Primary pores are difficult to recognize in the bone-bearing sandstone due to the high clay content. Exploded biotite fabric with secondary pores between biotite crystals in the basal sandstone (Figure 9.B) is indicative of calcite cement dissolution during later diagenesis. Such a diagenetic history makes differentiating primary pores from secondary pores difficult. Therefore, additional information is required to estimate burial depth.

Burial Depth. Schmidt and McDonald (1979) studied the relationship among porosity, compositional maturity, and burial depth in sandstones (Figure 27).

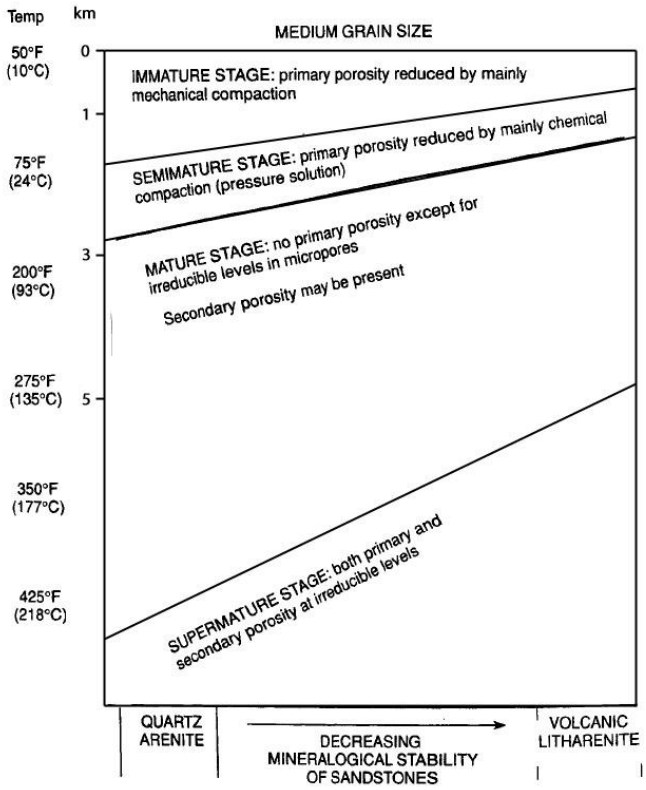


Figure 29. A schematic diagram showing the relationship between porosity evolution and burial depth (Modified from Schmidt and McDonald, 1979).

Since the bone-bearing sandstone is compositionally immature (feldspathic litharenite), most primary pores would have been destroyed at the burial depth of 2km.

The Bighorn basin is a nearby, analogous Laramide-style sedimentary basin located in Wyoming and Montana (Figure 1). Regional epirogenic uplift in Late Oligocene or Early Miocene initiated erosion (Bown, 1980), hence maximum burial depth occurred prior to Late Oligocene or Early Miocene time. The basin-fill model based on thermal parameters from Cretaceous rocks and oil well temperature data suggest that net aggradation to present day was approximately 2.7km, removing virtually all of the middle to late Tertiary rocks in the Bighorn basin (Hagen and Surdam, 1989). The

geothermal gradient ranges from 25°C/km to 32°C/km (Hagen and Surdam, 1989), suggesting that the maximum burial temperature at such a depth was close to 90°C.

Bone Microstructure

The fossils in the assemblage retain microstructures such as the Haversian system including osteonal lamina and Haversian canal and lacunae for osteocytes (Figure 11-12). Preservation of these microstructures requires: 1) inhibition of microbial attack, 2) close temporal association of collagen degradation and bone apatite alteration/growth, and 3) structural rigidity for preventing the effect of mechanical compaction. Although authigenic mineral precipitation is favorable for fossil preservation, displacive overgrowth of authigenic minerals can destroy fossil bone microstructures (Holz and Schultz, 1989).

Jans et al. (2004) reported that microbial attack is very common among archaeological bones regardless of climate. However, Trueman and Martill (2002) states that such structures (e.g. microbial/fungal boring and tunnels) are very rare among fossilized bones (N=350) spanning more than 350 million years, and covering a wide range of depositional environments. Thus, Trueman and Martill (2002) concluded that inhibition of early collagen degradation is necessary for fossil preservation. Lingham-Soliar (2010) shows dehydration and rehydration can increase survivability of collagen. Such rehydration can also introduce dissolved ions into the bone-collagen system. Since the hydroxyl group is thought to be shared by bone mineral and collagen (Pasteris et al., 2004), such fluid introduction not only increases survivability of collagen, but also aids alteration/overgrowth of bone minerals.

Displacive overgrowth of authigenic minerals can damage bone microstructures in fossils. For example, Holz and Schultz (1998) studied Brazilian Triassic fossils that show significant diagenetic modification such as "swelling", "distortion" and "compression", and concluded such modification occurred in early diagenetic stage where lithostatic pressure is low and rate of calcite precipitation is high. Holz and Schultz (1998) also states that the degree of diagenetic alteration among the fossils studied is highly variable: from undeformed to highly deformed with various mineral replacement. Early precipitation (pedogenesis to the vadose zone of eogenesis) of calcite in the bone-bearing sandstone is recorded in the concretions (Figure 19); however, bone microstructures do not include any evidence for displacive overgrowth of authigenic minerals. Thus, the rate of calcite precipitation in the bone-bearing sandstone was relatively low.

Using an average geostatic pressure gradient of 244bars/km (Boggs, 2003, p. 358) and estimated burial depth (2.7km), lithostatic pressure at the maximum burial depth is estimated as 660bars. Permineralization of the fossil bone is observed in larger bone (i.e. humerus and rib fragment of unknown dinosaur), and such mineral can act as physical support of the fossilized bone macro-structure. However, many smaller pores (i.e. cancellous bone pores and Haversian canals) are not perminerallized, suggesting perminerallization is not the only mechanism inhibiting the effect of mechanical compaction. Possible sources of structural rigidity of fossil bones include bone apatite overgrowth and authigenic mineral in nano-voids. Further analyses are necessary in order to test the effect of such changes.

Alteration of Bone Minerals

Bones are composed of protein fibers (collagen and minor non-collagenous proteins), mineral crystals often referred to as bioapatite (carbonated hydroxy-apatite similar to mineral dahllite; $Ca_{10}(PO_4,CO_3)_6(OH)_2$), and water (e.g. Trueman et al., 2008). Although bioapatite is commonly referred to as "hydroxapatite", various studies indicate bone apatite does not contain a significant amount of hydroxyl ion (e.g. Rey et al., 1995; Pasteris et al., 2004). Such unusual chemistry is possibly due to: 1) constant remodeling in living tissue and 2) increased collagen - bone mineral bonds by sharing OH-groups (Pasteris et al., 2004; Kohn and Law, 2006). Apatite in general can incorporate various cations and anions, which allow the organism to store elements necessary for various metabolisms (Skinner, 2000). Additionally, due to its extremely small crystal size (350-400Å x 350-400Å x 25-50Å (Weiner and Price, 1986)), bone mineral is highly soluble in most burial environments; hence crystal growth and/or alteration is required for bone preservation (Hubert, et al., 1996; Trueman and Tuross, 2002).

In contrast to modern bones, fossil bones contain no protein fiber or water and are mainly composed of fluoro-apatite (Hubert et al., 1996; Pasteris and Ding, 2009). Such fluoro-apatite is often referred to as francolite and contains various amounts of carbonate and other anions. Since the solubility of fluoro-apatite is much lower than hydroxy-apatite, alteration of the bioapatite into fluoro-apatite is suspected to have an important role for fossil preservation (e.g. Trueman and Tuross, 2002; Nemliher et al., 2004). Additionally, fossil bones are composed of a fine-grained cryptocrystalline mixture of predominantly apatite and a small amount of calcite (collophane) (Nesse, 2000, p. 348).

X-Ray Diffraction. The XRD spectra of apatite and bone (modern versus fossil) are highly variable due to the substitutions in the crystal lattice (e.g. LeGeros, 1980; Rogers et al., 2010). LeGeros et al. (1967) demonstrates the variety of XRD spectra due to different carbonate concentration within apatite structrue; (211) and (112) peaks merge into one broad peak when CO_3 concentration is 15%, and (300) peak shifts toward smaller d-spacing. Rogers et al. (2010) demonstrates that XRD spectra for unheated modern bones include a broad peak around 2.7Å instead of three peaks of (211), (112) and (300) due to the lower crystallinity of bone apatite.

The XRD data suggest that the most abundant mineral in the fossilized bone is either hydroxyl-apatite or fluoro-apatite; both are equally likely based on comparison with the ICDD database. Sharp peaks for (211), (112) and (300) on the XRD spectra (Figure 20) suggest that high crystallinity of apatite in fossil bone as well as lower concentration of carbonate in comparison to contemporary bones (Brophy and Nash, 1968; LeGeros et al., 1967; Wright and Schwarcz, 1996; Rogers et al., 2010). Therefore, the bone apatite in the fossils studied is diagenetically altered.

Fossil Color. Early precipitation of calcite (e.g. exploded fabric of biotite crystals, Fugure 9B) suggests the pore fluid in the soil was alkaline. Archaeological bones in alkali soil often show cream to white color since metal ions such as $Fe^{3+, 2+}$ and Mn^{2+} are trapped in carbonate precipitates (Turner-Walker, 2008). However, the fossilized bones analyzed in this study show reddish brown color, which is an indication of acidic soil environment in archaeological bones (Turner-Walker, 2008). Thus, the color of bone is indicative of further diagenetic alteration rather than early burial

environment. Such reaction may be ionic exchange under acidic diagenetic conditions, which is evidenced by oversized pores and grain alterations. LeGeros et al. (1980) reports that incorporation of Mn^{7+} (as MnO^{4-}) within synthetic apatite causes a brown color, suggesting the brown color may be due to uptake of MnO^{4-} by the bone mineral in later diagenesis.

An alternative cause of fossil color is the authigenic minerals within fossil bone matrix. Hubert et al. (1996) states reddish brown color of fossilized bone in the Jurassic Morrison Formation is due to Fe-oxide and hydroxide (e.g. hematite and goethite) microcrystals precipitated in microfractures of bones. However, the XRD spectrum (Figure 20) did not support presence of hematite within bone matrix. Instead, siderite is present within the fossil bones suggesting the reddish brown color of fossil bone is due to siderite in micro- and nanovoids.

Authigenic Mineral Precipitation

The authigenic mineral precipitates present within the fossilized bone include siderite, clay minerals and barite. Hematite is also present in the concretion matrix and some pores in cancellous bone. In order to discuss the spatial distribution of the authigenic mineral within fossil bone, terminology by Barker et al. (1997) is adopted in this thesis. Such classification include; megavoids (external to the surface of bones), macrovoids (large voids that are internal to the bone fabric), mesovoids (voids within bone fabric, up to a few mm^3), microvoids (smaller voids within bone tissue, few tens of microns in diameter), and nanovoids (void within the bone fabric produced by the decomposition of organic matter, 1-2 microns in diameter) (Figure 30).

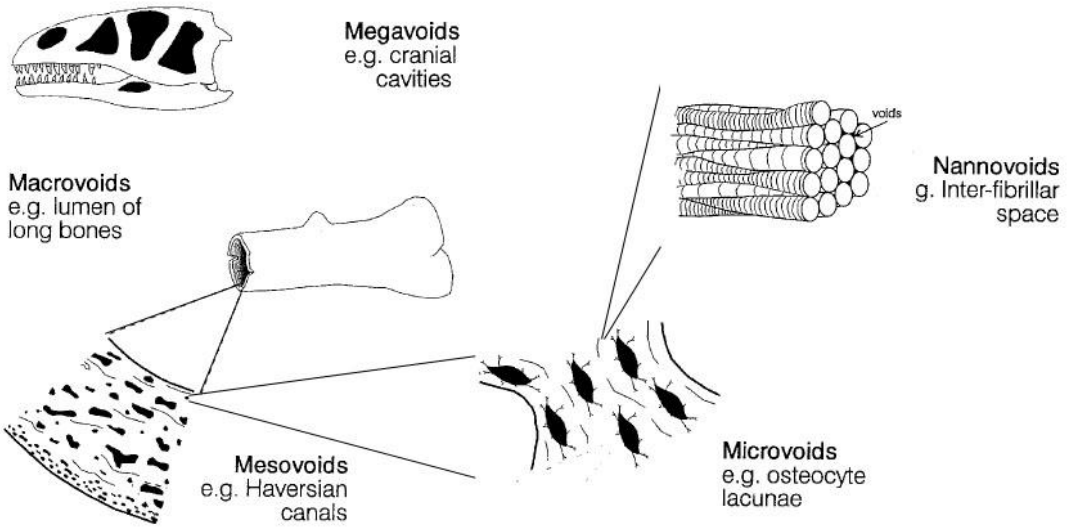


Figure 30. Schematic diagram of the void classification (modified from Barker et al., 1997)

Siderite. Siderite is present within macrovoids as a part of concretionary matrix (Figure 11). Siderite crystals are not observed by microscopy (both petrographic and SEM) within the bone matrix. However, fossil bones react with weak acid, suggesting carbonate is present in nanovoids. The XRD spectra of fossil bones (Figure 20) include three significant peaks at around 2.79, 2.78 and 2.77Å. The peaks at 2.79 and 2.77 are likely (211) and (112) peaks of bone apatite based on comparison with the ICDD database; hence the peak at around 2.78Å is interpreted as a peak for an authigenic mineral. Since the position of the peak is closest to the known peak of siderite among carbonate minerals (2.8Å according to Mindat), the authigenic mineral is interpreted as siderite.

Clay Minerals. The presence of lithic fragments within macro- and mesovoids indicates that the fossil bones were under the influence of pore fluid infiltration, which

transported lithic fragments and clay detrital clay minerals in sandstone matrix to void spaces within fossil bones. Such fluid movement is likely more prevalent in earlier diagenesis where primary pores are still present. However, presence of secondary pores suggests such clay mineral movement can take place in later diagenetic stages as well. Thus, clay mineral precipitation could take place in any diagenetic stage.

Some bone fragments observed within mesovoids indicate alteration of the bone mineral to clay mineral (Figure 12E). Such clay minerals are likely product of telogenesis, which include decrease in pressure and temperature, meteoric fluid, and surface weathering.

Barite. Barite is present in some mesovoids of fossilized bones and absent within sandstone and concretion matrices. In modern bone assemblages (Amboseli National Park, Kenya), barite is the second most common authigenic mineral in the bone pores, and precipitation of barite is especially common in the Haversian canals (Trueman et al., 2004). Various associations of barite with fossilized bone have been reported; crystals found outside of the bone (e.g. Matsubara, 1980), as a main constituent of permineralization (e.g. Wings, 2004), and trace amounts within permineralization (e.g. Holz and Schultz, 1998).

Since barite precipitates under various pore-fluid conditions, it is not a good indicator of pore-fluid geochemistry (Wings, 2004). However, presence of barite suggests that pore fluid was depleted in Ca^{2+}; hence precipitation of barite may be coupled with calcite or dolomite precipitation. Such conditions developed repeatedly during pedogenesis, eogenesis and telogenesis. Thus, the earlier precipitation

interpretation is better supported since 1) telogenetic precipitation of gypsum is seen nearby (in the Makoshika State Park) outcrops of the Hell Creek and Tullock outcrops, and 2) studies of both archaeological (Trueman et al., 2004) and ancient (Wings, 2004) fossilized bones suggest early precipitation of barite.

Hematite. Hematite occurs in the concretion matrix within the fossilized bone (Figure 13A), and such concretion forms on the surface of the bone and within macrovoids. Curtis and Coleman (1986) states that iron oxides and hydrated iron oxides are most probably secondary oxidation products when seen in ancient concretions. Since the hematite concretion include siderite matrices, the hematite concretion is interpreted as a product of siderite oxidation.

Geochemistry of Pore-Fluids

Wings (2004) suggests pore-filling authigenic minerals such as calcite and barite precipitate in anoxic and slightly alkaline conditions. Such conditions apply to some authigenic minerals found in this study; however, pore-fluid geochemistry is not constant throughout diagenesis as indicated by coexisting indicators of alkaline (e.g. calcite precipitation) and acidic (e.g. secondary pores) conditions. Therefore, evolution of pore-fluid geochemistry needs to be interpreted.

The indications for diagenetic fluid chemistry include the carbonate minerals, mineral dissolution/alteration, clay minerals, and other authigenic mineral precipitations. Since diagenetic environments change due to burial/uplift, diagenesis is subdivided into four stages; 1) pedogenesis - soil diagenesis; 2) eogenesis - early diagenesis; 3)

mesogenesis - deep burial; 4) telogenesis - diagenesis due to uplift including surface weathering.

Table 3. Fluid conditions in each diagenetic stage.

Diagenetic Stage	Fluid condition	Temperature
Pedogenesis	Meteoric and soil pore-fluid	Surface Temperature
Eogenesis	Vadose and Phreatic	Low Temperature (<65°C)
Mesogenesis	Brine	High Temperature (>65°C)
Telogenesis	Brine - Meteoric water	Low Temperature (<65°C)

The interpreted paragenetic sequence is summarized on the Figure 31.

Pedogenesis. Pedogenesis is the shallowest/earliest diagenetic stage characterized by soil formation. It includes biological and physical weathering. Considering the general duration of soil formation, this stage persists up to 10^4 years. In the penecontemporaneous (at or near depositional interface) realm, alteration of volcanic rock fragments and feldspar into kaolinite take place (Pittman, 1979; Boggs, 2003, p.401-404) due to biological/microbiological activity and acidic meteoric water.

Other authigenic minerals precipitated in this stage include carbonate minerals. As exploded fabric of biotite crystals (Figure 9.B) indicates, the pore fluid in soil was alkaline; such alkalinity is due to biological activity (i.e. plants and microbes). These early carbonate precipitates are not preserved in the sandstone matrices unless the pore-fluid interaction was restricted by other diagenetic mineral precipitation.

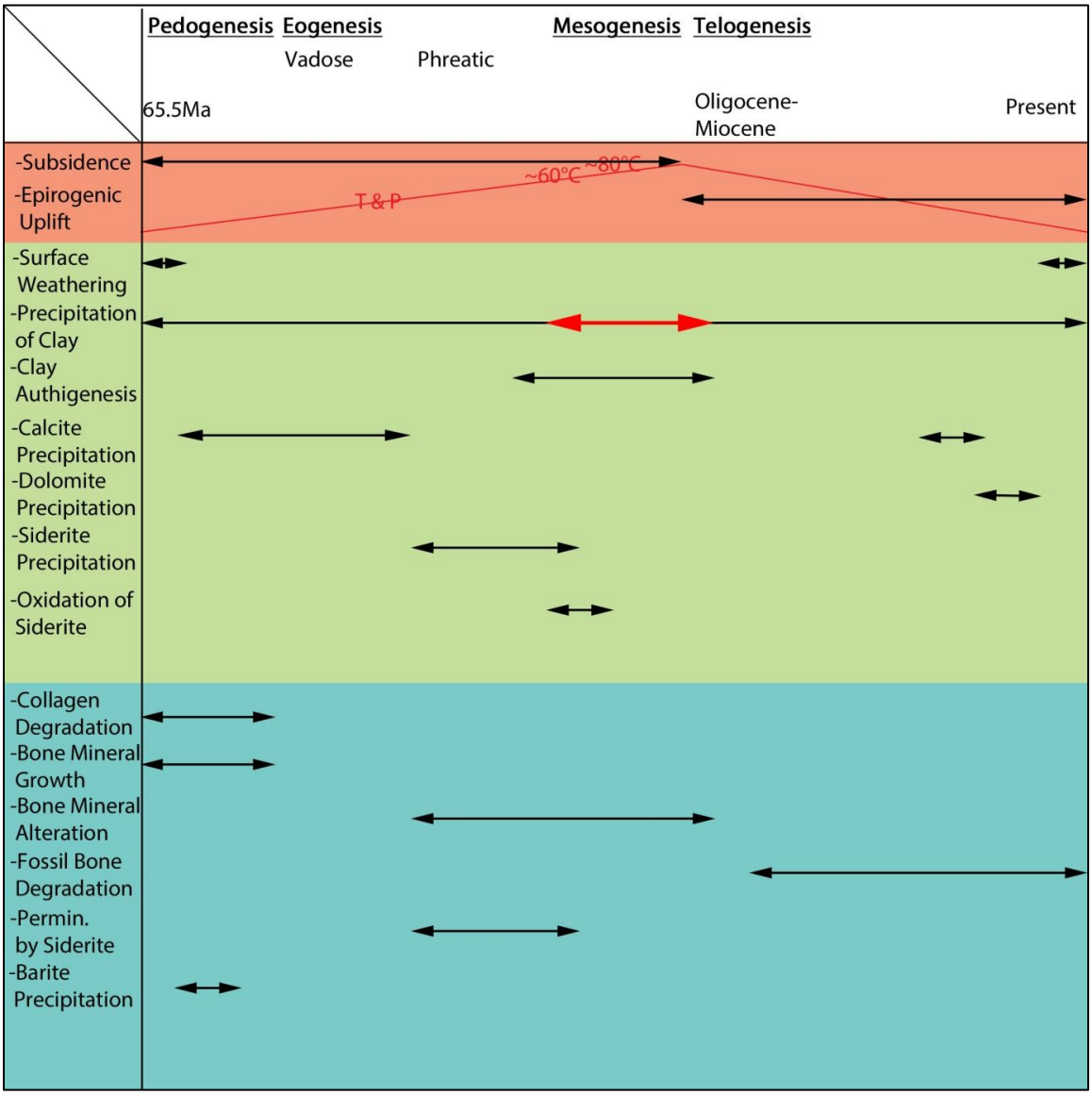


Figure 31. Summarized paragenetic sequence. The x-axis of the diagram represents the time (not scaled).

Pyrite is known to precipitate during pedogenesis where iron is present in the fluid and sulfur is provided by collagen degradation (Pfretzschner, 2001a). Such release of sulfur is related to decay of organic material. However, pyrite is not present in the bone or sandstone, suggesting either ion was consumed by other reaction such as precipitation of siderite (iron) or gypsum (sulfur). Alternatively, pyrite could have

precipitated and altered to other minerals such as hematite. However, the inclusion in the hematite concretion is siderite instead of pyrite; hence, early precipitation of pyrite probably did not take place in the bone-bearing sandstone.

Pfretzschner (2001b) suggests that precipitation of iron oxide (i.e. hematite) by changing the oxidation state from ferrous to ferric iron in early diagenesis preserves histologic structures; such hematite precipitation shows no replacement of adjacent bone and only takes place with the presence of collagen. Pfretzschner (2004) defines "early diagenesis" as "diagenesis when collagen is still present in bones". Such condition lasts usually for few 10^3 to 10^4 years (Kohn and Law, 2006; Tuken et al., 2008); hence, such "early diagenesis" takes place during pedogenesis, as used in this study. Osteonal lamellae are observed in thin-section (Figure 16); however, SEM and elemental mapping do not show concentration of iron outlining the osteonal lamellae (Figure 23). Thus, early precipitation of iron oxide for the preservation of histologic structure did not take place; the lamella observed in the thin-section is due to the fabric of fossil bone minerals rather than authigenic precipitation.

Eogenesis. Eogenesis can be subdivided into vadose (unsaturated) zone and phreatic (saturated) zone due to the characteristics of fluid condition. Vadose zone by definition includes the pedogenic zone; however, the use of vadose zone here is restricted to the diagenetic zone below the pedogenic zone and above the phreatic zone. This zone is characterized by lower biological activity in comparison to pedogenic zone and unsaturated fluid condition.

Calcite precipitated in the vadose zone exhibit meniscus fabric, which appears as partial grain coating (James and Choquette, 1983). The SEM micrograph (Figure 21.B) exhibits partial grain coating by calcite on a quartz grain suggesting vadose cementation. Such evidence supports repeated wetting/drying of bones pore-fluid containing Ca^{2+} ion in the vadose zone. Also, precipitation of calcite suggests the pore-fluid in the vadose zone was alkaline.

The siderite grain coatings precipitated in the phreatic zone exhibit isopachous fabric (James and Choquette, 1983). The grain coatings in the light concretion (Figure 14B) exhibit isopachous fabric indicating the pore-fluid in the phreatic zone was alkaline and rich in Fe^{2+} rather than Ca^{2+}. Thus, siderite precipitation was followed by the formation of concretions on fossil bones since the concretions enclose such grain coatings. In order to distinguish these two siderite phases, more sophisticated techniques (such as isotope and trace element analyses) need to be utilized.

Mesogenesis. Mesogenesis is known as the zone of most extensive diagenesis due to the elevated pressure and temperature; for example, an increase of 10°C can double or triple the reaction rate (Hunt, 1979, p. 127). Such conditions increase solubility of silicates and lithic fragments, but decrease solubility of carbonate and also favor precipitation of denser and less-hydrous minerals (Boggs, 2003, p. 370). Additionally, Fe^{2+} and Mn^{2+} are less hydrated at burial temperatures above 60°C, favoring precipitation of siderite and ankerite rather than calcite (Boggs, 2003, p. 370). Clay authigenesis takes place in the diagenetic temperature range of 55-200°C, releasing various cations such as

K^+, Fe^{3+} and Mg^{2+} (Freed and Peacor, 1989). Thus, clay authigenesis could aid formation of siderite in earlier mesogenesis.

Considering the high organic content of the bone-bearing sandstone, pore fluid later in this stage was likely acidic due to degradation of organic material. Although raised burial temperature decreases solubility of carbonate, acidic pore-fluid will still dissolve carbonate minerals. Accelerated degradation of organic matter can take place in the diagenetic temperature of 75-80°C (Boggs, 2003, p. 373). Therefore, most of the secondary pores were produced during later mesogenesis. Since siderite is soluble under such acidic conditions, oxidation of siderite concretion to hematite should predate such acidic conditions. Thus, the timing of the siderite oxidation is between formation of siderite concretion (eogenesis, phreatic zone) and acidic pore-fluid condition (mesogenesis, 75-80°C). Oxidation of siderite may be mediated by microbial metabolism (Webber et al., 2006).

Telogenesis. Throughout telogenesis, the lithostatic pressure and temperature gradually decrease due to the epirogenic uplift in the region. Decrease in temperature limits the production of organic acid by breakdown of organic molecules, hence the pore-fluid pH will rise. The reprecipitated carbonate cement in the bone-bearing sandstone matrix is indicative of such conditions; the carbonate cements in the bone-bearing sandstone are interpreted as telogenetic origin due to the presence of secondary pore in the same sandstone matrix. Carbonate also fills the cracks near the concretion.

Once exposed, surface weathering processes can destroy fossilized bones fairly quickly. Such weathering processes include infiltration by acidic meteoric water, freeze-

thaw cycle, and UV radiation (sunlight). Biological activities, such as phosphate acquisition by plant roots, can destroy post-uplift near-surface fossil bones as well. As a result of these processes, bones on the surface of the assemblages are fractured and fragmented along with original fabric (parallel to the shaft) and weathered to white color. The weathering process also causes alteration of unstable minerals such as feldspar and rock fragments, producing clay minerals.

Diagenetic Microenvironment within Fossilized Bones

Hematite concretions occur both inside (i.e. marrow cavities) and outside of the fossil bones. The grains contained in the concretion exhibit similar characteristics (i.e. angular fine-sand sized grains, grain coating within the siderite matrices, etc.). Also the mesovoids in the fossil bones contain detrital grains. Such observations suggest the fossilized bones were not isolated from surrounding sandstone.

Although the fluid conditions were likely the same, the presence of barite in mesovoids is unique to the fossil bone. This may be related to localized ionic conditions related to early collagen degradation; degradation of collagen releases sulfur, an element required for barite precipitation.

CONCLUSION

The depositional environment of the sandstone including the fossil assemblage studied is interpreted as crevasse splay. Taphonomy of the same fossil assemblage was not fully understood due to the small sample size. However, based on the data collected, the assemblage can be interpreted as an attritional accumulation rather than episodic. The bimodal pattern of breakage and variable weathering are consistent with the crevasse splay depositional environment.

The originally hypothesized sequence of diagenetic events affecting skeletal material included: 1) early precipitation of carbonate, 2) alteration of bone minerals, and 3) modification of bone pore spaces. The early precipitation of carbonate was supported by petrography, XRD and SEM/EDS. Carbonate minerals precipitated in these diagenetic stages were calcite and siderite, and they were preserved in siderite/hematite concretion. The alteration of bone apatite was supported by XRD and SEM/EDS. Such alteration is likely associated with early dehydration and rehydration of collagen, which introduces various ions in the bone mineral - collagen interface. The pore spaces in the bone were not affected by physical compaction; however, precipitaition of authigenic minerals (i.e. siderite, hematite, barite, and clay minerals) was very common. Such precipitates are useful for interpreting the pore-fluid condition during diagenesis.

This study demonstrates that petrography, XRD and SEM/EDS together can help deciphering the diagenetic history of fossilized bones. In order to maximize the information, not only the fossil bones, but surrounding rocks need to be analyzed because surrounding rocks record different sets of diagenetic processes such as calcite

precipitation in the vadose zone, siderite precipitation in the phreatic zones, acidic pore-fluid condition in mesogenesis. Concretions are known for extraordinary preservation including soft part anatomy of the fossils (Cope and Curtis, 2000). Additionally, concretions restrict the interaction between grains and pore-fluid; hence concretions may contain unique sets of geochemical information not found in fossil bones and surrounding sedimentary rocks. Such an approach is helpful for interpreting evolution of pore-fluid geochemistry, which is not constant throughout diagenetic history. Better understanding of diagenesis helps interpreting geochemical/paleontological information preserved in fossil bones including biomolecular and isotopic data. Although bone microstructures are well preserved in the fossil bones studied, they are diagenetically altered as indicated by petrography, SEM and XRD. Thus, biomolecular and isotopic data are likely indicative of diagenetic conditions instead of biological signals (e.g. taxonomic or metabolic information) of the organism.

Future Study

The sample size for taphonomic analysis was not large enough. Thus, the same methods need be applied to bone assemblages with larger sample size in order to understand the relationship between taphonomic data and diagenetic data in future. Furthermore, taphonomic and diagenetic modes vary within the Hell Creek Formation. Therefore, comparison of taphonomic and diagenetic data among various Hell Creek fossil assemblages may reveal more thorough relationship between depositional environment and/or evolution of pore-fluid geochemistry in regional scale.

Fluoridation of the fossil bones is only partially supported by this study due to the detection limit of the EDS. Since fluoridation may increase the chemical stability of bone mineral, chemical composition of bone should be investigated further with more sophisticated tools such as electron microprobe. Such study may reveal the degree of fluoridation in fossil bones and importance of such alteration for better preservation of bioclasts in rock record.

Although it is impossible to imitate the time scale of actual fossilization, actualistic experiments are required to confirm the geochemical models supported this study (and previous studies). Confirming the relationship between introduction of ions by dehydration and rehydration of collagen and alteration/growth of bone apatite in particular would be a step-forward for bone diagenesis since such result would reassure the importance of early (first 10^3-10^4 years) diagenesis.

Siderite found in the concretion exhibits two separate phases; isopachous grain coating and concretion matrix. For better understanding of diagenetic history, isotope analysis could be utilized to interpret the timing of such siderite precipitation.

Lastly, smectite-illite ratio in the mixed layered clay, oxygen isotope ratio, and vitrinite reflectance can be used for estimating maximum diagenetic temperature (Freed and Peacor, 1989; Boggs, 2006, p. 151). Even though the XRD software (DMSNT) used for this study was not compatible with such analysis, similar analysis can be conducted for better maximum diagenetic temperature analysis.

REFERENCES CITED

REFERENCES CITED

Barker, M.J., Clarke, J.B. and Martill, D.M., 1997, Mesozoic reptile bones as diagenetic windows, Bulletin de la Societe Geologique de France, v. 168, p. 535-545

Boggs, S. Jr., 2003, Petrology of sedimentary rocks, Blackburn Press, Caldwell, NJ, 707p.

Boggs, S. Jr., 2006, Principles of sedimentology and stratigraphy, 4th edition, Pearson Prentice Hall, Upper Saddle River, NJ, 662p.

Briggs, D.G., 2003, Paleobiology II, Blackwell Publishing, Malden, MA, 583p.

Brophy, G.P. and Nash, J.T., Compositional, infrared, and X-ray analysis of fossil bone, American Mineralogist, v. 53, p. 445-454

Collins, M.J., Nielsen-Marsh, C.M., Hiller, J., Smith, C.I., Roberts, J.P., Prigodich, R.V., Wess, T.J., Csapo, J., Millard, A.R., and Turner-Walker, G., 2002, The survival of organic matter in bone: a review, Archaeometry, v. 44, p. 383-394

Cope, J.C.W. and Curtis, C.D., 2000, Palaeobiology meets geochemistry: concretions as tombs, Journal of the Geological Society, London, v. 157, p. 163-164

Currey, J.D., 2002, Bones: structure and mechanics, Princeton University Press, Princeton, NJ, 436p.

Curtis, C.D. and Coleman, M.L., 1986, Control on the precipitation of early diagenetic calcite, dolomite and siderite concretions in complex depositional sequences, Special publication; the Society of Economic Paleontologists and Mineralogists, v. 38, p. 23-33

Daniel, J.C. and Chin, K., 2010, The role of bacterially mediated precipitation in the permineralization of bone, Palaios, v. 25, p. 507-516

Fastovsky, D.E., 1987, Paleoenvironments of vertebrate-bearing strata during the Cretaceous-Paleogene transition, Eastern Montana and Western North Dakota, Palaios, v. 2, p. 285-295

Freed, R.L. and Peacor, D.R., 1989, Geopressured shale and sealing effect of smectite to illite transition, The American Association of Petroleum Geologists Bulletin, v. 73, p. 1223-1232

Gonzalez Riga, B.J. and Astini, R.A., 2007, Preservation of large titanosaur sauropod in overbank fluvial facies: a case study in the Cretaceous of Argentina, Journal of South American Earth Science, v. 23, p. 290-303

Goodwin, M.B., Grant, P.G., Bench, G., and Holroyd, P.A., 2007, Elemental composition and diagenetic alteration of dinosaur bone: distinguishing micron-scale spatial and compositional heterogeneity using PIXE, Paleogeography, paleoclimatology, paleoecology, v. 253, p. 458-476

Hagen, E.S., and Surdam, R.C., 1989, Thermal evolution of Laramide-style basins: constrainings from the Northern Bighorn basin, Wyoming and Montana, thermal evolution of Laramide-style basins; methods and case histories, p. 277-295

Hedges, R. E. M., 2002, Bone diagenesis: an overview of processes, Archaeometry, v. 44, n. 3, p. 319-328

Holz, M., and Schultz, C.L., 1998, Taphonomy of the south Brazilian Triassic herpetofauna: fossilization mode and implication for morphological studies, Lethaia, v. 31, p. 335-345

Hunt, J.M., 1979, Petroleum geochemistry and geology, W.H. Freeman and Company, San Francisco, CA, 617p.

Hubert, J.F., Panish, P.T., Chure, D.J., and Prostak, K.S., 1996, Chemistry, microstructure, petrology, and diagenetic model of Jurassic dinosaur bones, dinosaur national monument, Utah, Journal of sedimentary research, v. 66, p. 531-547

Jans, M.M.E., Nielsen-Marsh, C.M., Smith, C.I., Collins, M.J., and Kars, H., 2004, Characterisation of microbial attack on archaeological bone, Journal of Archaeological Science, v. 31, p. 87-95

Johnson, K.R. and Hickey, L.J., 1990, Megafloral change across the Cretaceous/Tertiary boundary in northern Great Plain and Rocky Mountains, U.S.A., Geological Society of America Special Paper, v. 247, p. 433-444

Johnson, K.R., Nichols, D.J., and Hartman, J.H., 2002, Hell Creek Formation: a 2001 synthesis, Geological Society of America Special Paper, v. 361, p. 503-510

James, N.P. and Choquette, P.W., 1983, Diagenesis 9 - limestones -the meteoric diagenetic environment, Geoscience Canada, v. 10, p. 161-194.

Kaye, T.G., Gaugler, G., and Sawlowicz, Z., 2008, Dinosaurian soft tissues interpreted as bacterial biofilms, PLoS one, v. 3, n. 7, e2808

Kohn, M.J. and Law, M., 2006, Stable isotope chemistry of fossil bones as a new paleoclimate indicator, Geochimica et Cosmochimica Acta, v. 70, p. 931-946

LeGeros, R.Z., Trautz, O.R., LeGeros, J.P., Klein, E., and Shirra, W.P., 1967, Apatite crystallites: Effects of carbonate on morphology, Science, v. 155, n. 3678, p. 1409-1411

LeGeros, R.Z., Taheri, M.H., Quirolgico, G.B. and LeGeros, J.P., 1980, Formation and solubility of apatite: effects of some cationic substitution, 2nd International Congress on Phosphorous Compounds, p. 89-102

Lingham-Soliar, T. and Glab, J., 2010, Dehydration: a mechanism for the preservation of fine detail in fossilized soft tissue of ancient terrestrial animals, Paleogeography, Paleocoimatology, Paleoecology, v. 291, p. 481-487

Lund, S.P., Hartman, J.H., and Banerjee, S.K., 2002, Magnetostratigraphy of interfingering upper Cretaceous-Paleocene marine and continental strata of the Williston Basin, North Dakota and Montana, Geological Society of America Special Paper, v. 361, p. 57-74.

Marshall, D.J., 1988, Cathodoluminescence of geological materials, Unwin Hyman, London, UK, 146p.

Matsubara, S., 1980, Barite and carbonate-apatite constituting fossil dinosaur bone in sandstone from Berivotra, Madagascar, Bulletin of the National Science Museum Series C, v. 6, p. 27-31

McCabe, Peter J., 1984, Depositional environments of coal and coal-bearing strata, Special Publication of International Association of Sedimentologists, v. 7, p. 13-42

Miall, A.D., 2007, The geology of fluvial deposits: facies, basin alalysis, and petroleum geology, Springer, 598p.

The Mineral and Locality Database (Mindat), <www.mindat.org>, last accessed on 05/01/2013

Moore, D.M. and Reynolds, R.C. Jr., 1997, X-ray diffraction and the identification and analysis of clay minerals, 2nd edition, Oxford University Press, New York, NY, 378p.

Morad, S., 1998, Carbonate cementation in sandstones: distribution patterns and geochemical evolution, Special Publication of International Association of Sedimentologists, v. 26, p. 1-26.

Nemliher, J.G., Baturin, G.N., Kallaste, T.E., and Murdmaa, I.O., 2004, Transformation of hydroxyapatite of bone phosphate from the ocean bottom during fossilization, Lithology and Mineral Resources, v. 39, p. 468-479

Nesse, W.D., 2000, Introduction to Mineralogy, Oxford University Press, New York, NY, 442p.

Parry, W.T., 2011, Composition, nucleation, and growth of iron oxide concretions, Sedimentary Geology, v. 233, p. 53-68.

Pate, F.D., Hutton, J.T., and Norrish, K., 1989, Ionic exchange between soil solution and bone: toward a predictive model, Applied Geochemistry, v. 4, p. 303-316

Pasteris, J.D., Wopenka, B., Freeman, J.J., Rogers, K., Valsami-Jones, E., Hauwen, J.A.M. and Silva, M.J., 2004, Lack of OH in nanocrystalline apatite as a function of degree of atomic order: implications for bone and biomaterials, Biomaterial, v. 25, p. 229-238.

Pasteris, J.D. and Ding, D.Y., 2009, Experimental fluoridation of nanocrystalline apatite, American Mineralogist, v. 94, p. 53-63

Person, A., Bocherens, H., Saliege, J.-F., Paris, F., Zeitoun, V., and Gerard, M., 1995, Early diagenetic evolution of bone phosphate: an X-ray diffractometry analysis, Journal of Archaeological Science, v. 22, p. 211-221

Person, A., Bocherens, H., Mariotti, A., and Renard, M., 1996, Diagenetic evolution and experimental heating of bone phosphate, Paleontology, Paleoclimatology, Paleoecology, v. 126, p. 135-149.

Pfretzschner, H.-U., 2001a, Pyrite in fossil bone, Neues Jahrbuch fuer Geologie und Paleontologie, v. 220, p. 1-23

Pfretzschner, H.-U., 2001b, Iron oxides in fossil bone, Neues Jahrbuch fuer Geologie und Paleontologie, v. 220, p. 417-429

Pfretzschner, H.-U, 2004, Fossilization of Haversian bone in aquatic environments, C.R. Palevol, v. 3, p. 605-616

Pfretzschner, H.-U., 2006, Collagen gelatinization: the key to understand early bone-diagenesis, Palaeontographica Abteilung A: Palaeozoologie-stratigraphie, v. 278, p. 135-148

Pittman, E.D., 1979, Recent advances in sandstone diagenesis, Annual Reviews in Earth and Planetary Sciences, v. 7, p. 39-62

Reading, H.G., 1996, Sedimentary environments: processis, facies and stratigraphy, London, Blackwell science, 688p.

Rey, C., Miquel, J.L., Facchini, L., Legrand, A.P. and Glimcher, M.J., 1995, Hydroxyl groups in bone mineral, Bone, v. 16, p. 583-586

Rogers, K., Beckett, S., Kuhn, S., Chamberlain, A. and Clement, J., 2008, Contrasting the crystallinity indicators of heated and diagenetically altered bone mineral, Palaeogeography, Palaeoclimatology, Palaeoecology, v. 296, p. 125-129

Russel, D.A. and Manabe, M., 2002, Synopsis of the Hell Creek (uppermost Cretaceous) dinosaur assemblage, Geological Society of America Special Paper, v. 361, p. 169-176

Rust, B.R., 1978a, A classification of alluvial channel systems, Memoir - Canadian Society of Petroleum Geologists, v. 5, p. 187-198

Rust, B.R., 1978b, Depositional models for braided alluvium, Memoir - Candadian Society of Petroleum Geologists, v. 5, p. 605-625

Schmidt, V. and McDonald, D.A., 1979, The role of secondary porosity in the course of sandstone diagenesis, SEPM special publication, v. 26, p. 175-207

Schweitzer, M.H., Johnson, C., Zocco, T.G., Horner, J.R., and Starkey, J.R., 1997, Preservation of biomolecules in cancellous bone of Tyrrannosaurus rex, Journal of Vertebrate Paleontology, v. 17, p. 349-359

Schweitzer, M.H., Marshall, M., Korron, K., Bohle, D.S., Busse, S.C., Arnold, E.V., Barnard, D., Horner, J.R., and Starkey, J.R., 1997, Heme compound in trabecular bone, Proceedings of the National Academy of Science, v. 94, p. 6291-6296

Schweitzer, M.H., Wittmeyer, J.L., Horner, J.R., and Toporski, J.K., 2005, Soft-tissue vessels and cellular preservation in Tyrannosaurus rex, Science, v. 307, p. 1952-1955

Schweitzer, M.H., Wittmeyer, J.L., and Horner, J.R., 2007, Soft tissue and cellular preservation in vertebrate skeletal elements from the Cretaceous to the present, Proceedings of the Royal Society B, v. 274, p. 183-197

Schweitzer, M.H., 2011, Soft tissue preservation in terrestrial Mesozoic vertebrates, Annual Review of Earth and Planetary Science, v. 39, p. 187-216

Sheehan, P.M, Fastovsky, D.E., Hoffmann, R.G., Berghaus, C.B. and Gabriel, D.L., 1991, Sudden extinction of the dinosaurs: latest Cretaceous, Upper Great Plains, U.S.A., Science, v. 254, p. 835-839

Shipman, P., 1981, Life history of a fossil, an introduction to taphonomy and paleoecology, Harvard University Press, Cambridge, MA, 222p.

Shoup, B.E., 2001, Sedimentology and taphonomy of a shell bed assemblage from the upper Cretaceous (Maastrichtian) Hell Creek Formation of eastern Montana, Master's thesis, Montana State University, 66p.

Smith, D.G., 1983, Anastomosed fluvial deposits: modern examples from western Canada: Special Publication of International Association of Sedimentologists, v. 6, p. 155-168

Skinner, H.C.W., 2000, In praise of phosphates, or why vertebrates chose apatite to mineralize their skeletal elements, International Geology Review, v. 42, p. 232-240

Surdam, R.C., MacGowan, D.B., and Dunn, T.L., 1989, Diagenetic pathways of sandstone and shale sequences, Contributions to Geology, v. 27, n. 1, p. 21-31

Trueman, C.N., and Tuross, N., 2002, Trace elements in recent and fossil bone apatite, Phosphates: geochemical, geobiological, and materials importance, Reviews in Mineralogy and Geochemistry, v. 48, p. 489-521

Trueman, C.N., and Martill, D.M., 2002, The long-term survival of bone: the role of bioerosion, Archaeometry, v. 44, p. 371-382

Trueman, C.N., Behrensmeyer, A.K., Tuross, N., and Weiner S., 2004, Mineralogical and compositional changes in bones exposed on soil surface in Amboseli National Park, Kenya: diagenetic mechanisms and the role of sediment pore fluids, Journal of Archaeological Science, v. 31, p. 721-739

Trueman, C.N., Palmer, M.R., Field, J., Privat, K., Ludgate, N., Chavagnac, Valerie, Eberth, D.A., Cifelli, R., and Rogers, R.R., 2008, Comparing rates of

recrystallisation and the potential for preservation of biomolecules from the distribution of trace elements in fossil bones, C.R. Palevol, v. 7, p. 145-158

Turner-Walker, G., 2008, The chemical and microbial degradation of bones and teeth, Advances in Human Paleopathology, p. 3-29.

Tuken, T., Vennemann, T.W. and Pfretzschner, H.-U., 2008, Early diagenesis of bone and tooth apatite in fluvial and marine settings: constraints from combined oxygen isotope, nitrogen and REE analysis, Palaeogeography, Palaeoclimatology, Palaeoecology, v. 266, p. 254-268

United States Geological Survey (USGS) Open File Report 01-041, <http://pubs.usgs.gov/of/2001/of01-041/htmldocs/flow/>, last accessed on 05/01/2013

Vuke, S.M. and Colton, R.B., 1998, Geologic map of the Glendive 30' x 60' quadrangle eastern Montana and adjacent North Dakota, Montana Bureau of Mines and Geology Open File, n. 371

Walker, J.D., and Geissman, J.W., 2009, 2009 Geologic time scale, Geological Society of America, doi: 10.1130/2009.CTS004R2C

Webber, K.A., Achenbach, L.A. and Coates, J.D., Microorganisms pumping iron: anaerobic microbial iron oxidation and reduction, Nature Reviews Microbiology, v. 4, p. 752-764

Weiner, S. and Price, P.A., 1986, Disaggregation of bone into crystals, Calcified Tissue International, v. 39, p. 365-375

White, P.D., Fastovsky, D.E. and Sheehan, P.M., 1998, Taphonomy and suggested structure of the dinosaurian assemblage of the Hell Creek Formation (Maastrichtian), eastern Montana and western North Dakota, Palaios, v. 13, p. 41-51

Wings, O., 2004, Authigenic minerals in fossil bones from the Mesozoic of England: poor correlation with depositional environments, Palaeogeography, Palaeoclimatology, Palaeoecology, v. 204, p. 15-32

Wood, J.M., Thomas, R.G. and Visser, J., 1988, Fluvial processes and vertebrate taphonomy: the Upper Cretaceous Judith River Formation, south-central Dinosaur Provincial Park, Alberta, Canada: Paleogeography, Paleoclimatology, Paleoecology, v. 66, p. 127-143

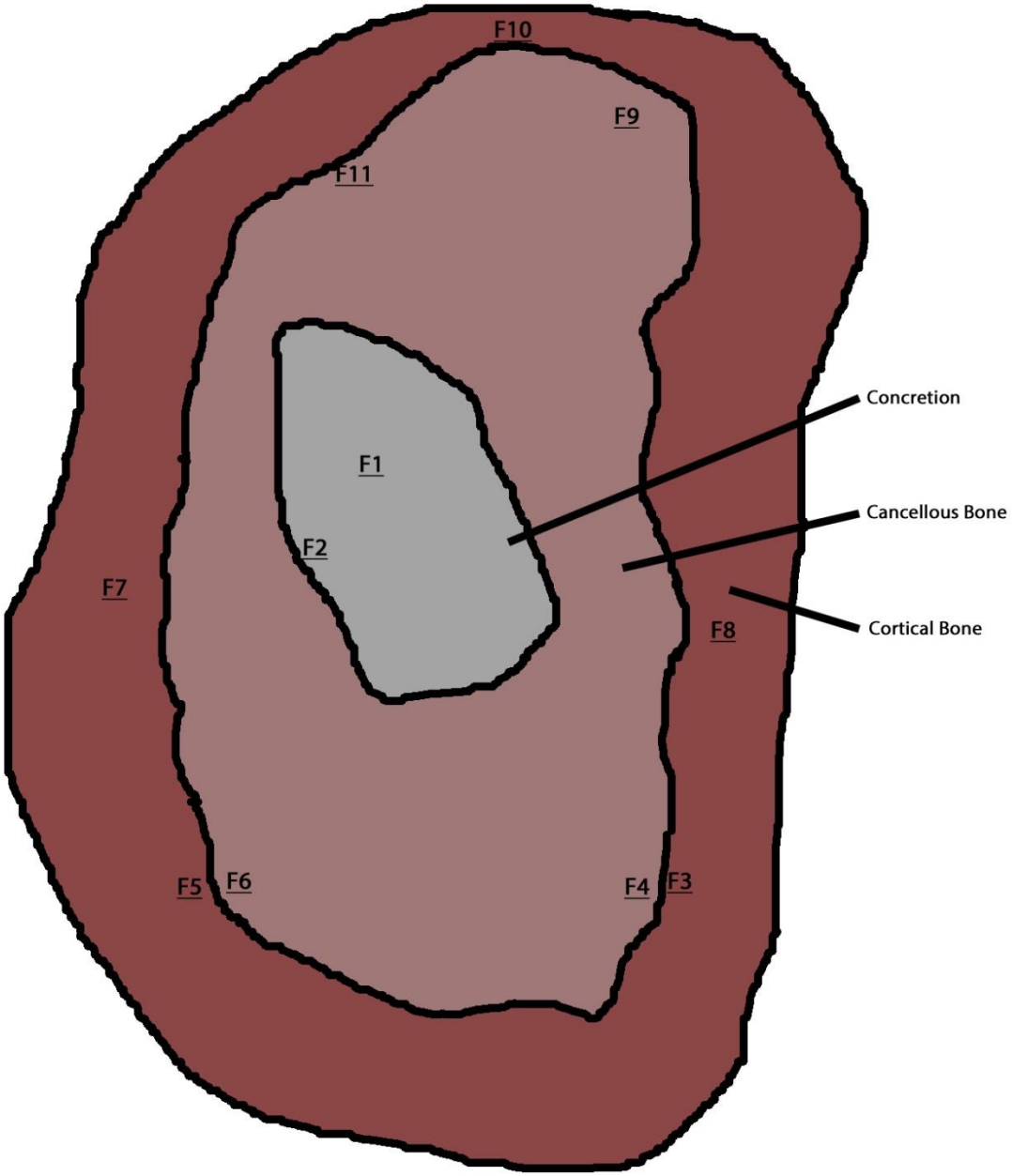
Wright, L.E. and Schwarcz, H.P., 1996, Infrared and isotopic evidence for diagenesis of bone apatite at Dos Pilas, Guatemala: palaedietary implication, Journal of Archaeological Science, v. 23, p. 933-944

Zaleha, M.J., 1988, The Hell Creek Formation (Maastrichtian), Glendive area, Montana: sedimentology, paleoenvironments, and provenance and their stratigraphic and taphonomic implication, Master's thesis, Ohio University, 137p.

APPENDICES

APPENDIX A

MAP OF THE FEMUR FRAGMENTS


F10
F9
F11
F1
F2
F7
F8
F5
F6
F4
F3
Concretion
Cancellous Bone
Cortical Bone

APPENDIX B

LIST OF THIN-SECTIONS AND TREATMENTS

	Sample #	femur p.	Comments	Stain
Concretion	C1		Concretion directly above the humerus	
	C1 C		same as above	Calcite
	C1 F		same as above	Ferrous iron
	C2		Sandstone - Concretion boundary	
	C2 S		same as above	Calcite
	C2 F		same as above	Ferrous iron
Rib	R1		Rib fragment	
	R2		Adjacent to R1	
Femur	F1	C	concretion filling femur	
	F1 C	C	same as above	Calcite
	F2	C	Adjacent to F1	
	F2 C	C	same as above	Calcite
	F3	L Right	Spongy toward center	
	F4	L Right	Spongy toward center	
	F5	L Left	Spongy toward center	
	F6	L Left	Adjacent to F5	
	F7	M Left	Friable	
	F8	M Right	very Friable (broken into multiple pieces)	
	F9	U Right	Friable	
	F10	T Center	very friable	
	F11	U Left	Friable, sandstone attached	
Bone-bearing Sandstone	S1		Bone-bearing sandstone	
	S1 K		same as above	K-spar
	S2		Bone-bearing sandstone	
	S2 K		same as above	K-spar
Basal Sandstone	BS 1		Basal sandstone	
	BS 1 K		same as above	K-spar
	BS 2		Basal sandstone	
	BS 2 K		same as above	K-spar
Concretion on Rib	RC 1		big concretion with some bone pieces	
	RC 1 C		same as above	Calcite

RC 1 F		same as above	Ferrous iron
RC 2		Adjacent to RC1	
RC 2 C		same as above	Calcite
RC 2 F		same as above	Ferrous iron